Chapter 5
Lipid Bilayer-Membrane Protein Coupling

Lipid organization in membranes forms liquid crystalline structures. Membrane proteins, like all other proteins, exist with solid structure, if not generally, then at least relate to the structure of lipid membranes. The coupling between these two different structural components is rather complicated. Biological membranes are dynamical macromolecular assemblies, composed of lipid bilayers with embedded bilayer-spanning proteins that move within the plane of the membrane. This seminal membrane concept was originally proposed as the fluid mosaic membrane model [82]. A lipid bilayer's primary function is to serve as a semipermeable barrier for solute movement between different, membrane-separated fluid compartments. This barrier function depends on the bilayer's hydrophobic core being a poor "solvent" for polar solutes. The bilayer permeability coefficient for solute X (P_X) can be approximated as:

$$P_X = \frac{\alpha_X D_X}{\zeta}, \tag{5.1}$$

where α_X is the solute partition coefficient between the bilayer core and the aqueous phase, D_X is the solute diffusion coefficient in the bilayer core (which varies little among small solutes [29]), and ζ denotes the bilayer hydrophobic thickness ($\sim$30 Å for hydrocarbon-free bilayers [54, 81], or 40–60 Å for hydrocarbon-containing bilayers [16]). Experimental results obtained for a wide variety of solutes show that P_X is proportional to X, as approximated by the solutes' oil/water partition coefficient [29, 70, 90], and that the solute diffusion coefficient in the bilayer core is similar to the diffusion coefficient in bulk hydrocarbons (10^{-6} to 10^{-5} cm^2/s [79]).

The elucidation of the role of membrane proteins requires a specific mechanism of lipid regulation of the membrane protein function which is extremely important, but poorly understood so far. The free kinetic characteristics of membrane proteins inside a lipid bilayer are imaginary. In reality, the dynamical properties of membrane proteins are a result of various contributions from their interactions with host phospholipid layers and other integral constituents such as other membrane proteins, hydrocarbons, cholesterols, etc. The background dielectric properties also play important roles. In this chapter, we focus on different components that

M. Ashrafuzzaman and J. Tuszynski, *Membrane Biophysics*,
Biological and Medical Physics, Biomedical Engineering,
DOI: 10.1007/978-3-642-16105-6_5, © Springer-Verlag Berlin Heidelberg 2012

contribute to the strength of the hydrophobic coupling of the membrane proteins with the host phospholipid bilayer. Several novel analytical and numerical techniques will be introduced to correctly address this important problem. Although we have developed a theoretical model published earlier, which aims to explain the related experimental phenomena, we have also presented the results here to describe the problem in a comprehensive fashion.

The experimental study focused on a few ion channel phenomena which will be used as tools to address the problem. We also discuss some of the lipid- membrane protein interactions using molecular dynamics (MD) simulations. The powerful MD methodology mimics the cell membrane with most of the constituents within the membrane simulated by computer modeling. This helps understand the dynamics and energetics of various compartments, especially considering them to be independent of other compartments in membranes in real time which is experimentally almost impossible to investigate due to the complex organization of biological systems. It is also necessary to emphasize that MD can never provide absolute values of the physical parameters which should fit the biological environment but it can often provide enough information to help understand the phenomena involved.

5.1 Lipid Membrane–Membrane Protein Coupling Due to Membrane Elasticity

5.1.1 Definition of Elasticity

According to the fluid mosaic model [82], lipids freely move on the membrane surface like a fluid. This is well-known, as a liquid crystalline structure. Liquid crystalline membranes exist in different thermotropic phases. This was discussed in Chap. 3. Within any specific phase, the structure requires specific organization of the lipid molecules, and such organization raises the possibility of the membrane having certain distinguishable biophysical properties. Elasticity is claimed to be one of the few most important ones. However, the question arises whether this type of elasticity resembles the elasticity of a solid state material, which follows Hooke's law. If any object quickly regains its original shape and dimensions following the withdrawal of the force creating the deformation in the first place, with the molecules or atoms of the object returning to their initial state of stable equilibrium, the object is considered to be elastic and it obeys Hooke's law. Specifically, in mechanics, Hooke's law of elasticity is an approximation that states that the amount of deformation (represented by strain) is linearly related to the force causing the deformation (represented by stress). This hypothesis best fits with the extension of a spring due to the suspension of a load at the bottom (see Fig. 5.1). If the load is removed, the extended spring returns to its original structure and length.

The mathematical form of the spring's distortion follows the equation

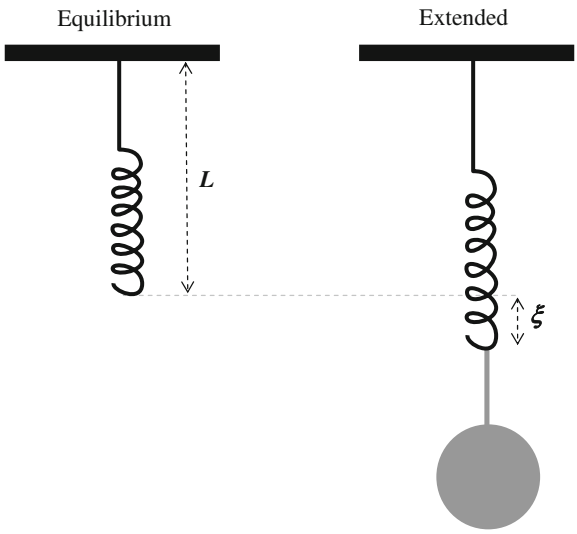

Fig. 5.1 A vertically suspended spring with an equilibrium length L extends to its new length L+ξ due to a load W [kg] suspended at the bottom of the spring

$$F = -k\xi, \tag{5.2}$$

where F is the restoring force exerted by the material, and k is the force constant (spring constant in the case of a spring). If $\xi \ll L$, the spring behaves as a harmonic oscillator. Here, F and ξ are measured using the conventional units of force (newtons) and linear dimension (meters), respectively.

The associated energy stored in the spring following the Eq. 5.2 is given by

$$U = \frac{1}{2}k\xi^2. \tag{5.3}$$

One of the important conditions of Hooke's law is that the body returns to its equilibrium state instantaneously as soon as the suspended weight is removed, which means that in the case of the above-mentioned spring, it will regain its original length L soon after the weight W is taken away from its attachment point.

Does the lipid membrane behave like a spring which can be extended or deformed without breaking its molecular organization or specific structure? Does the membrane return to its original length and shape once the membrane extending or deforming force is withdrawn? Does the membrane follow Hooke's law; represented either by the restoring force F (see Eq. 5.2) or elastic energy U (see Eq. 5.3)? These are some intriguing questions, which membrane biophysicists have been trying to answer during over almost a half-century since the publication of the famous paper by Helfrich on the elastic behavior of the lipid membrane [37]. Various groups of researchers have attempted to address the bilayer's elastic problems using different techniques which will be discussed later in this chapter. However, first we wish to mention a generally accepted fact about lipid membranes which states that they form liquid

crystalline structures (see for example [64]). It is still not clear whether some or all of the elastic properties are satisfied by a liquid crystalline membrane. Despite the lack of any cross-examination between the membrane's elasticity and its liquid crystalline nature, a group of scientists have already asserted the absolutely elastic nature of liquid crystalline lipid bilayers. Furthermore, membrane regulation of most of the membrane protein dynamics and general functions have also been concluded to be governed mainly by the bilayer elastic properties and geometries like lipid curvature profiles, etc. However, in addition to the elasticity of membranes, the electric properties of lipids, membrane proteins, and other participating constituents are very important but much less studied and understood. In this chapter, we provide an in-depth analysis of these aspects as well. First, we describe the membrane's elastic properties and related aspects using some experimental studies considering a few ion channel phenomena.

5.1.2 The Membrane's Elasticity Helps It to be Flexible: A Study Using the Gramicidin A Channel as a Tool

We first focus on an ion channel, that is, a channel formed by a small peptide gramicidin A; these channels are used as probes which hydrophobically couple with host lipid membranes. The advantage of using gramicidin A peptides to investigate membrane elastic properties is that they usually make channels which are smaller in length than the normal thickness of phospholipid bilayers (see Fig. 5.2). The length of gramicidin A channels can be varied by changing the lengths of gramicidin A peptides. It is worth mentioning that gramicidin A channels can also be artificially synthesized, such that their length may exceed the bilayer thickness.

Based on generally accepted schematic diagrams depicting gramicidin A channels inside lipid membranes (see Fig. 5.2), it is clear that the main condition for the formation of stable channels is a hydrophobic mismatch between bilayer thickness and gramicidin A channel lengths, which needs to be geometrically adjusted. Before we explore this issue, we need to understand how a bilayer deformation may occur. Due to the bilayer's elastic nature, we can consider the presence of an unlimited number of virtual springs attached between two lipid monolayers. This has been schematically shown in Fig. 5.3. The springs oscillate and maintain harmonic motion, keeping the average thickness of the bilayer uniform unless any membrane proteins or other bilayer structure-deforming agents appear in the vicinity; both inside the bilayer's hydrophobic core and in the hydrophobic/hydrophilic boundaries on both sides. Any bilayer deformation due to an independent bilayer elastic property must be much smaller than the thickness of the bilayer. Additionally, any deformation is certainly instantaneous. The elasticity-originated instantaneous thickness fluctuations follow Hooke's law and a related equation of motion for a harmonic oscillator which was stated earlier. However, the physics of the problem changes when there happens to be a molecular force acting to induce a substantial permanent deformation which

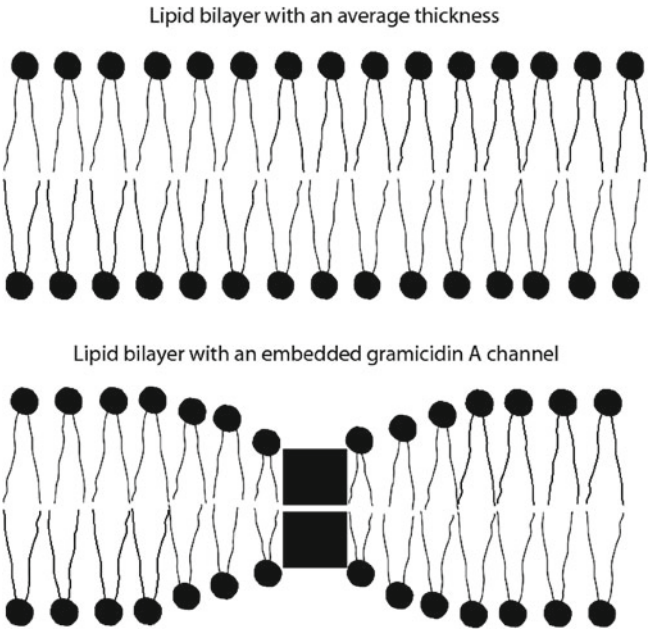

Fig. 5.2 The bilayer deforms near the gramicidin A channels where the channels are considered to be coupled with the host bilayer incurring an energetic cost [13]. The *upper panel* shows a lipid bilayer without any integral membrane protein, which is why the bilayer exists with an average bilayer thickness d_0 (see Fig. 4.2). The *lower panel* shows a bilayer with an integral gramicidin A channel. For simplicity, we use two blocks in the figure to represent a gramicidin A dimer. The channel's length l can differ, depending on the type of monomers participating in constructing the channel (see Fig. 4.2). d_0 is the unperturbed thickness of the bilayer, and is on the order of 4–5 nm in hydrocarbon-containing lipid bilayers. The value of d_0 depends highly on the type of hydrocarbons residing inside the bilayer. In the model lipid membrane construction, decane or squalene are usually used. Decane accounts for a relatively thicker bilayer than squalene. By varying the lipid acyl chain lengths, the bilayer thickness can be varied. The channel length l is on the order of 2 nm depending on the number of amino acid sequences involved in constructing the gramicidin A monomers. The channels form a rigid structure which means that the lengths are almost constant

might act as a molecular force transducer. The presence of ion channels inside a lipid membrane sometimes takes the form of a molecular force transducer, such as gramicidin A, in a lipid bilayer (see Fig. 5.2). The gravitational push (for example by a drug) on the membrane, or a pull exerted on the lipid layers by integral membrane proteins due to their hydrophobic coupling with lipid layers, may create considerable permanent or stable deformations. These deformations may sometimes cause drastic effects, such as a local breaking in the bilayer structure, or an induction of substantial flow of ions through pores or channels. Figure 5.4 schematically illustrates the equilibrium condition which can take the deformed form presented in Fig. 5.2 for gramicidin A channel. It is important to understand whether bilayer elasticity can

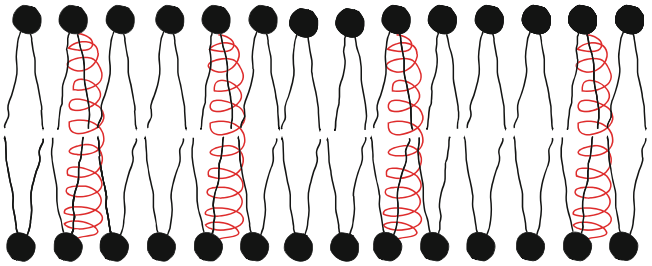

Fig. 5.3 Virtual springs (shown in *red*) are longitudinally attached to the two monolayers. For simplicity of presentation we have shown that those virtual springs are attached with lipid head group layers on each monolayer of the bilayer. The choice of the number and shape of the springs is arbitrary

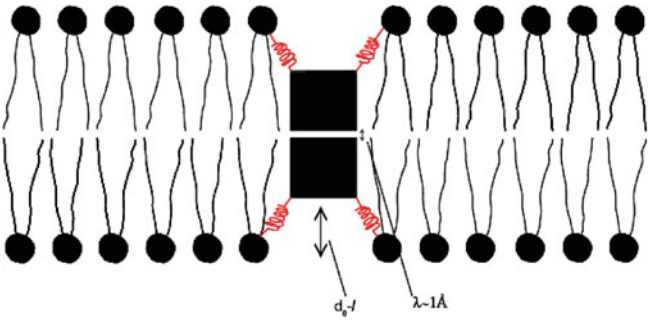

Fig. 5.4 A bilayer- integral gramicidin A channel coupling phenomenon is modeled here as a harmonic interaction. Any gramicidin A channel is attached to a lipid monolayer with many imaginary springs where any of these springs follows the motion of a harmonic oscillator following Eq. 5.2. Two gramicidin A monomers are attached to each other by hydrogen bonds and the monomer-monomer separation falls within $\lambda \approx 1$ Å or 0.1 nanometer (nm). To simplify the diagram we draw two blocks representing two gramicidin A monomers in this figure instead of showing them as spiral structures shown in Fig. 5.2

still be used as the main ingredient which causes the necessary energetic changes required for this type of mechanical deformation.

Since both channel formation and channel breaking are statistical processes, the geometrical adjustment of the free length $d_0 - l$ is a very temporary effect, but certainly not instantaneous. The bilayer's elastic nature can help it to deform to adjust with the channel's length so that a real physical binding between the lipid layers and the channel's longitudinal edges may happen. In the case of gramicidin A channels, we assume that if the channels try to extend linearly to compensate for the mismatch $d_0 - l$, the bonding at the center of the channel between two gramicidin A monomers will be broken, so that the gramicidin A channels will themselves be diluted into gramicidin A monomers. Instead, if the rather soft structured membrane exhibits a deformation near the channel, the problem can be solved and gramicidin A channels will show some stability. However, this requires a change of free energy due

to the membrane deformation, and many researchers proposed that the free energy change is contributed due to the elastic bilayer properties. We present here a detailed analysis of the bilayer's elastic energy, which arises from the consideration of the mechanical properties of the lipid bilayer. A spontaneous bending near the channel's edges (as diagrammed in Fig. 5.2) is a possible model. The crucial issue is to find the force which drives the lipid layers inward to bind with the channel's edges. Is it a harmonic energetic coupling as schematized in Fig. 5.4? If so, then we can model the bilayer-gramicidin A channel coupling through many virtual springs which will pull both of the lipid layers toward the channel's longitudinal edges. Each lipid layer then needs to spontaneously bend through a free length, which is proportional to $(d_0 - l)/2$ in each longitudinal edge of the channel, to satisfy the condition of the hydrophobic bilayer channel coupling as diagrammed in Fig. 5.2. The bilayer's elastic property certainly helps the monolayers to spontaneously bend (see Fig. 5.2), but since the bending is permanent, with a high level of stability proportional to the channel lifetime, the mechanism certainly falls outside simple harmonic coupling. In this case, the virtual springs presented in Fig. 5.4 need to compress by a length proportional to their equilibrium lengths. Therefore, the virtual springs do not just follow the motion of a harmonic oscillator (see Eq. 5.2), but rather, higher order anharmonic terms appear in the potential energy formula in addition to the harmonic oscillator terms (see Eq. 5.3).

The scientific arguments presented here clearly suggest that a brand-new formula is needed to describe bilayer channel coupling energetics, and one has to include both harmonic (originating from elastic properties) and anharmonic (originating from unknown properties) bilayer integral channel coupling terms. We discuss this in the next section, but first we address the existing bilayer channel coupling energetics based on the bilayer's mechanical properties, especially bilayer elasticity.

5.1.3 The Membrane's Elastic Property Contributes to the Membrane–Membrane Protein Coupling: A Study Using the Gramicidin A Channel as a Tool

The general or primary function of membrane proteins is to catalyze the selective transfer of material and information across biological membranes. In the case of catalyzing this transfer, membrane proteins undergo conformational changes, namely: (a) the opening/closing transitions in ion channels [72, 73, 88] and (b) the shift in substrate binding site accessibility in conformational carriers and ATP-driven pumps [87]. To the extent that these protein conformational changes involve the protein/bilayer interface, they will perturb the bilayer immediately adjacent to the protein [3, 20, 33, 42, 76], cf. Figs. 4.1 and 5.2. That is, protein conformational changes involve not only rearrangements within the protein, but also interactions with the environment, particularly with the host bilayer. This was discussed in an

earlier chapter and also earlier in this chapter. Here, we focus only on the energetic part.

The bilayer deformation, in general, incurs an energetic cost, ΔG^0_{def}, that contributes to the overall free energy difference ($\Delta G^{I->II}_{\text{tot}}$) between two different protein functional states (conformations), denoted here as I and II, respectively, such that

$$\Delta G^{I->II}_{\text{tot}} = \Delta G^{I->II}_{\text{prot}} + \Delta\Delta G^{I->II}_{\text{def}}, \tag{5.4}$$

where $\Delta G^{I->II}_{\text{prot}}$ denotes the energetic cost of the protein conformational change *per se* (including contributions from interactions with the environment, such as changes in the protein/solution interface, not considered in the protein-bilayer interactions) and $\Delta\Delta G^{I->II}_{\text{def}}$, the difference in bilayer deformation energy between protein conformations I and II ($\Delta\Delta G^{I->II}_{\text{def}} = \Delta G^{II}_{\text{def}} - \Delta G^{I}_{\text{def}}$). Consequently, the equilibrium distribution between the different protein conformations is given by:

$$K^I_{II} = \exp\left(-\frac{\Delta G^{I->II}_{\text{prot}} + \Delta\Delta G^{I->II}_{\text{def}}}{k_B T}\right), \tag{5.5}$$

where K^I_{II} denotes the equilibrium distribution coefficient between protein states I and II, T stands for the absolute temperature of the bilayer environment and k_B is Boltzmann's constant. If ΔG^0_{def} is significant, meaning $|\Delta G^0_{\text{def}}| > k_B T$, then $\Delta\Delta G^{I->II}_{\text{def}}$ may be sizable, such that the equilibrium distribution between different membrane protein conformations—and the kinetics of the conformational changes—could be modulated by the bilayer in which the proteins are embedded [3, 20, 33, 76].

The success of Eq. 5.1 in predicting small molecule permeability coefficients naturally leads to the notion of lipid bilayers being thin sheets of liquid hydrocarbons, stabilized by the lipid polar head groups, as implied in the original formulation of the fluid mosaic membrane model [82]. If that were the case, one would expect that $|\Delta G^0_{\text{def}}| \ll k_B T$, in which case membrane protein function would be little affected by changes in bilayer properties—except in cases where the interfacial surface charge densities vary [39, 59, 65]. However, lipid bilayers are not just thin sheets of liquid hydrocarbon; they are liquid crystals that exhibit both short- and long-range order [64]. By virtue of being liquid crystals, lipid bilayers also have elastic properties [27, 37], with material properties (average thickness, intrinsic monolayer curvature and elastic moduli) that can be manipulated by the adsorption of amphipathic compounds [13, 28, 58, 77, 80, 84, 93] and other ones. The permeability of small molecules across lipid bilayers given by Eq. 5.5 can, on a broader scale, become highly regulated by the hydrophobic coupling between the lipid bilayer and the bilayer-spanning membrane proteins. To address this hydrophobic coupling between the lipid bilayer and the membrane proteins-induced regulation, we have investigated here both experimentally and theoretically the energetics of gramicidin A channels in lipid bilayers with different thickness. To generalize the problem, later in this

chapter, we also investigate the functions of another structurally different channel produced by alamethicin peptides.

We have learned earlier that the gramicidin A channel is a linear dimer. The atomic resolution structure of this channel is well-established, with the channels being dimers of two right-handed, $\beta^{6.3}$-helical subunits [8, 46, 86]. The bilayer-spanning channels are formed by the reversible, trans-bilayer association of these $\beta^{6.3}$-helical monomers [68]:

$$M_{\text{left}} + M_{\text{right}} \underset{k_{-1}}{\overset{k_1}{\rightleftharpoons}} D, \tag{5.6}$$

where M and D denote gramicidin A monomers and dimers, respectively, and the subscripts denote monomers residing in each bilayer leaflet. Here, k_1 and k_{-1} are two rate constants determining the channel appearance rate ($f_{\text{gA}} = k_1 \cdot [M]^2$; with $[M]$ being the gramicidin A monomer concentration) and gramicidin A channel lifetime ($\tau = 1/k_{-1}$). Within limits, the channel structure is invariant when the lipid bilayer thickness is varied [45, 89], meaning that the gramicidin A channels are more rigid than the host bilayer. Consequently, when the bilayer's hydrophobic thickness is larger than the channel's hydrophobic length, as is the present case, the bilayer will adjust locally to match the channel length, which incurs an energetic cost corresponding to the bilayer deformation energy ΔG^0_{def}. When a channel disappears, a transition state is reached when two of the six H-bonds that stabilize the bilayer-spanning dimer are broken [26, 61], in which case the two subunits have moved a distance $\lambda+$, which may be slightly greater than the average length λ ($\approx$1.0 Å) of the bonds attaching two gramicidin A monomers in a gramicidin A dimer. The movement of the two subunits relative to each other is very complex, involving both a rotation and a lateral axial displacement [61]. For simplicity, here we focus on just the linear gramicidin A association/dissociation mechanism only.

Changes in ΔG^0_{def} will shift the equilibrium distribution between non-conducting gramicidin A monomers and conducting channels. Using Eq. 5.5, the dimerization constant for gramicidin A channel formation, K_D, is found as

$$K_D = \frac{[D]}{[M]^2} = \frac{k_1}{k_{-1}} = \exp\left(-\frac{\Delta G^0_{\text{prot}} + \Delta G^0_{\text{def}}}{k_B T}\right), \tag{5.7}$$

where ΔG^0_{prot} denotes the energetic contributions due to the channel subunit-subunit interactions. Here, $[D]$ is the concentration of dimeric gramicidin A channels. Because bilayer deformation energy ΔG^0_{def} varies as a function of the mismatch between the bilayer thickness and the gramicidin A channel length ($d_0 - l$), the bilayer responds to the deformation by imposing a disjoining force on the bilayer-spanning channels:

$$F_{\text{dis}} = -\left(-\frac{\partial}{\partial r}\Delta G^0_{\text{def}}\right). \tag{5.8}$$

This force can, in principle, be determined theoretically, although this requires a complicated numerical calculation. If we assume that ΔG^0_{prot} does not considerably respond to bilayer deformation, changes in F_{dis} will mainly be observable as changes in channel lifetime τ, which means that gramicidin A channels become molecular force transducers embedded in the lipid bilayers [5]. This is so because $\tau = 1/k_{-1}$, where k_{-1} is the dimer dissociation rate constant. The disjoining force alters k_{-1} by altering the activation energy for channel dissociation:

$$k_{-1} = \frac{1}{\tau_0} \cdot \exp\left(\frac{\Delta G^{\ddagger}}{k_B T}\right) = \frac{1}{\tau_0} \exp\left(-\frac{\Delta G^{\ddagger}_{\text{prot}} + \Delta\Delta G^{\ddagger}_{\text{def}}}{k_B T}\right), \tag{5.9}$$

where τ_0^{-1} denotes the frequency factor for the reaction, $\Delta\Delta G^{\ddagger}_{\text{def}}$ and $\Delta G^{\ddagger}_{\text{prot}}$ denote the difference in bilayer deformation energy and the protein transition energy, respectively, as the two subunits move apart by a distance $(\lambda^+ - \lambda)(\ll (d_0 - l))$ to reach the transition state for dimer dissociation, and $\Delta G^{\ddagger}$ is their sum. With some approximation in the case $(\lambda^+ - \lambda) \approx 0$ (ignoring the change in protein conformational energy before the actual event of the real dissociation) the following equation is found:

$$\Delta\Delta G^{\ddagger}_{\text{def}} \approx F_{\text{dis}} \cdot (\lambda^+ - \lambda). \tag{5.10}$$

The transition between a gramicidin A dimer (D) and monomer (M) and vice versa, via the intermediate energy state where the dissociation/association between two gramicidin A monomers ($D \leftrightarrow M$) happens, is illustrated in Fig. 5.5.

Based on the molecular dynamics simulation of gramicidin A in lipid bilayers considering an all-atom force field [2], we have gained an important insight into how a gramicidin A channel exists inside lipid bilayers. We observe here that at the binding site of the channel bilayer interface, the lipid head group region is more effectively regulating the lipid bilayer gramicidin A channel hydrophobic coupling. That is, the lipid head groups, due to their physical presence, compensate for the hydrophobic free length $(d_0 - l)$ between the bilayer thickness and the channel length in the channel bilayer coupling interface (see the illustration of the model in Fig. 5.2). The bilayer, however, exerts a restoring force F_{dis} on the two longitudinal edges of the gramicidin A channel to return it to its original thickness and, as a result, the gramicidin A dimer experiences destabilization. It finally dissociates from the bilayer, and gramicidin A monomers also dissociate from each other.

Calculation of the F_{dis} acting against the bilayer gramicidin A channel coupling has been a long-standing challenge, and the form of F_{dis} mainly depends on how one treats a lipid bilayer membrane, such as whether it is treated as equivalent to a perfect elastic body or as a liquid crystalline structure. Based on the theory of elastic bilayer deformation [38, 40, 66, 67] the bilayer deformation energy has been found to show bi-quadratic form in terms of $(d_0 - l)$ and intrinsic monolayer curvature c_0 parameters [55, 66, 67]

$$\Delta G^0_{\text{def}} = H_B \cdot (d_0 - l)^2 + H_X \cdot (d_0 - l) \cdot c_0 + H_C \cdot c_0^2, \tag{5.11}$$

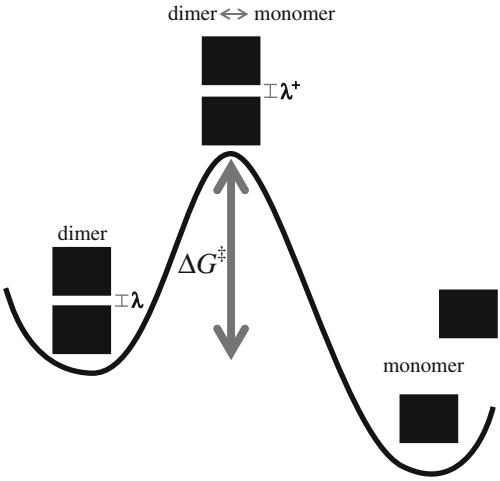

Fig. 5.5 Chemical kinetics illustration of the back-and-forth transitions between gramicidin A dimer (D) and monomer (M) states. The monomers in the far left energy well are bound to each other, but the monomers in the far right energy well are free from each other. The back-and-forth transition between dimer and monomer states happens near the central energy state. The gramicidin A monomer has been schematically shown as a block. As to the role of the energy state representing the left-most energy well, the contribution of the central energetic barrier with barrier height $\Delta G^{\ddagger}$ (*vertical double arrow*) relative to the energy well representing the dimer state is very important for the stability of the gramicidin A dimer (channel) state. The dissociation between the monomers may happen due to linear displacement, rotational bending, etc. To easily understand the problem, we analyze the dissociation mechanism here using only the linear displacement of the monomers along the channel length

where H_B, H_X and H_C are phenomenological elastic constants, depending mainly on the bilayer elastic properties, namely compression and bending moduli (for details see [13]). In this elastic model, the bilayer deformation free energy has been calculated based on the original proposal that for small deformations, the free energy consists of a layer-compression term, a splay-distortion term, and a surface-tension term, equivalent to the elastic free energy of a two-layer smectic liquid crystal with surface tension [40]. Consequently, F_{dis} follows a linear relationship with respect to $(d_0 - l)$ and c_0 [6, 13] such that

$$F_{\text{dis}} = -\left(-\frac{\partial}{\partial(d_0 - l)}\Delta G^0_{\text{def}}\right) = 2H_B \cdot (d_0 - l) + H_X \cdot c_0. \tag{5.12}$$

Increasing $(d_0 - l)$ and/or c_0 leads to an increase in F_{dis} which causes destabilization of gramicidin A channels following this general relation between F_{dis} and gramicidin A channel lifetime via the bilayer deformation energy contributions:

$$\tau \sim \exp\left(-\frac{\Delta\Delta G^{\ddagger}_{\text{def}}}{k_B T}\right) = \exp\left(-\frac{(\lambda^{+} - \lambda) F_{\text{dis}}}{k_B T}\right) \tag{5.13}$$

F_{dis} here follows from Eq. 5.12 in the elastic bilayer consideration.

In this elastic bilayer deformation energy calculation, the decomposed local bilayer compression and monolayer bending energy densities are often calculated considering the bilayer as an almost perfect elastic body. Equation 5.11 provides only the quadratic energy form of the mismatch $d_0 - l$, which is the harmonic energy coupling term (Eq. 5.3). This energy term does not consist of any anharmonic terms, which are highly needed especially in the case of having a considerable value of $d_0 - l$. Consequently, the lack of presence of nonlinear terms other than the linear term (proportional to $d_0 - l$) in the value of F_{dis} makes the form of F_{dis} in Eq. 5.12 incomplete and scientifically incorrect. This has been explained in detail in an earlier section, as well as in ([11] in Chap. 4). Therefore, a general form for F_{dis} must be formulated, using a totally different scientifically acceptable model, considering all general properties of the lipid bilayer and integral membrane proteins. We have done so using a screened Coulomb interaction model for calculating the hydrophobic bilayer-membrane protein coupling energy by including electrical properties of the lipids and membrane proteins ([11] in Chap. 4). We explain briefly below.

5.2 Lipid Membrane–Membrane Protein Coupling Due to Electrical Properties of Lipids and Proteins

In Sect. 5.1 we have discussed how the membrane's elastic properties raise the possibility of conditional mechanical energetic coupling between lipid layers and integral membrane proteins. We have also found that although the mechanical property of lipid layers (or generally, the bilayer elasticity) provides important contributions to the membrane functions, there are even more important biophysical properties, namely the electrical properties of the membrane constituents and the integral membrane proteins that generate primary effects on most of the membrane transport properties ([11] in Chap. 4). Based on this latter publication, it is clear that a traditional mechanical energetic coupling between the bilayer and membrane proteins does not contribute the primary regulatory effects on membrane proteins. Instead, the electrical energetic coupling does so.

5.2.1 Screened Coulomb Potentials and Lennard–Jones Interactions Between Peptides on Ion Channels and Lipids in the Membrane: A Study Using Gramicidin A Channel as a Tool

Using specific 'elastic parameters' in a fluid-like membrane is a good first-order approximation that works well within the limitations of a linear theory. However,

in order to extend the applicability of the theory to a non-linear regime, we propose to use the screened Coulomb interaction approximation instead of using the form of energy (Eq. 5.11) found from elastic considerations of the bilayer model. This screened Coulomb interaction approach has often been used in condensed matter physics as the so-called Thomas–Fermi approximation [9] as well as in biophysics for interacting systems of charged biomolecules in solution employing traditional Debye screening to account for the presence of water and ions, first introduced in the Debye-Hückel model [22]. Also, zwitterionic lipids having a dipole moment provide support for calculating localized (in the intermediate range) interaction energies between channel-forming peptides and nearby lipid head group regions in a manner equivalent to a free energy profile of interacting charged-zwitterionic lipid layers using the Debye-Hückel theory [60]. Here, we wish to mention that the presence of aqueous ions in the outer leaflet of the bilayer still leaves room for head group dipoles to show considerable localized charge effects in the inner region where channel lipid interactions take place. Moreover, the bilayer's spontaneous bending near channels (see Fig. 5.2) is obtained by finding the energy required to bend a straight charged chain where the screened Coulomb interactions lead to high values of induced stiffness [69], which is an example where the elastic model [38, 40] requires an extension to a nonlinear regime. The interaction energy between a gramicidin A channel and a host bilayer has been calculated based on experimentally observable parameters, such as bilayer thickness d_0 [16], lipid head group cross-sectional area [35], channel length l [41], lipid charge q_L [1, 75], and dielectric parameters of the lipid bilayer core [71], etc. Bilayer elastic parameters appear in the screened Coulomb interaction as secondary ingredients. In this screened interaction we assume that the gramicidin A channel couples with the lipid bilayer through a deformation of the bilayer at the channel bilayer interaction interface (see Fig. 5.2). Considering that the gramicidin A channel length is smaller than the thickness of the bilayer, the channel extends its Coulomb interaction toward lipids sitting on the bilayer's resting thickness. The gramicidin A channel directly interacts with the nearest-neighbor lipid (lp1) by the Coulomb interaction and this lipid interacts directly with its next-nearest-neighbor lipid (lp2) but this second lipid experiences an interaction with the channel which is screened due to the presence of the channel's nearest-neighbor lipid; a first-order term in the extension of V_{sc} (see Eq. 5.14). The interaction between the third-nearest-neighbor lipid (lp3) and the channel is screened by both the nearest- and next-nearest-neighbor lipids (the second-order term in the extension of V_{sc}). Figure 5.6 illustrates this in a diagrammatic view. The chain peptide-lipid interaction can be better explained by the curvilinear model diagram in Fig. 5.7, but the real condition is that the peptides interact with lipids in all directions on each monolayer leaflet. The general form of the screened Coulomb interaction is as follows:

$$V_{\mathrm{sc}}(\boldsymbol{r}) = \int d^3k e^{(i\boldsymbol{k}\cdot\boldsymbol{r})} V_{\mathrm{sc}}(\boldsymbol{k}), \tag{5.14}$$

where the screened Coulomb interaction in Fourier space is given by [9].

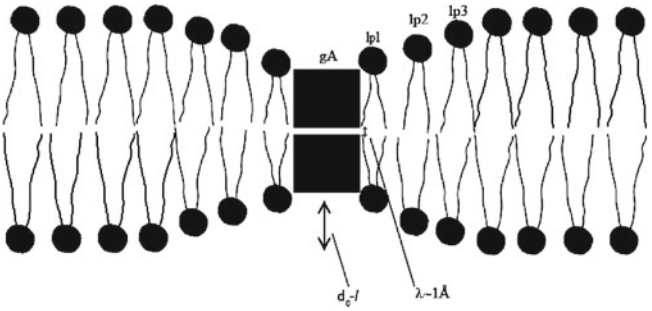

Fig. 5.6 Gramicidin A monomer (gA) and lipids on each monolayer make a chain (with chain reaction) with continuous bending until the equilibrium membrane thickness is reached. A gA monomer interacts with lp1 (direct Coulomb interaction which is the zeroth-order term in the expansion of the screened Coulomb interaction, Eq. 5.14), with lp2 (first-order screened Coulomb interaction), with lp3 (second- order screened Coulomb interaction), etc. The interactions extend to all directions on each lipid monolayer surface

$$V_{\rm sc}(\boldsymbol{k}) = \frac{V(\boldsymbol{k})}{1 + \frac{V(\boldsymbol{k})}{2\pi k_B T} n}, \tag{5.15}$$

where $V(k) \approx (1/\epsilon_0\epsilon_r) q_{\rm gA} q_L / k^2$ (in two-dimensional Fourier space) is the direct Coulomb interaction between particle 1 (gramicidin A monomer with effective charge $q_{\rm gA}$) and particle 2 (the gramicidin A monomer's nearest-neighbor lipid, with an effective charge on its head group region, q_L). Here, ϵ_0 is the dielectric constant in vacuum and ϵ_r is the relative dielectric constant (~2) [17] inside the membrane. The wave number is $k \approx 2\pi/a$, and a is the lattice constant or the closest distance over which a lipid head group can approach the gramicidin A channel's center of mass. The condition is better presented in the schematic 2D diagrams in Figs. 5.6 and 5.7. For simplicity, we assume $a = r_{\rm LL}$, the average lipid-lipid distance, which is about 7.7 Å [35]. n denotes the density e.g., lipid density $\sim 1/60\,\text{Å}^2$. $k_B T \approx 1.38 \times 10^{-23}$ J/K (at 300 K). $n/(2\pi k_B T) \approx 6.4 \times 10^{17}/\text{J Å}^2$, or $n \approx 3.84 \times 10^{19}/$ J (in general). Let us consider $q_{\rm gA} q_L \approx f q_{\rm gA}^2$, f ($\approx q_L/q_{\rm gA}$, assumed to be $\ll 1$) is the ratio of effective charges in lipid and in protein (gramicidin A monomer).

The screened Coulomb interaction (see Eqs. 5.14 and 5.15) underscores that the bilayer-gramicidin A channel mismatch may control the stability of the gramicidin A channel which is already dealt with in the order of the expansion of the interaction potential (through the number of lipids involved in the screening phenomenon). When there is no hydrophobic mismatch, the zeroth-order term (direct Coulomb interaction) in the expansion of Eq. 5.14 is to be the only one considered.

The binding energy between two gramicidin A monomers can be expressed as:

$$U_{gA,gA}(r) = U_{\rm LJ} + U_{\rm coulomb}(r), \tag{5.16}$$

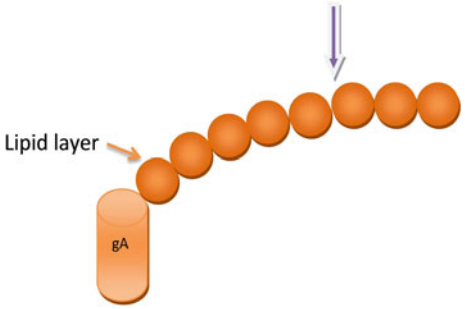

Fig. 5.7 Gramicidin A monomer (gA) in a channel is assumed to find a lipid (just the head group is schematically shown) on the perturbed region of the bilayer next to it with a bare Coulomb interaction, but the next-neighboring lipid with the first-order screened Coulomb interaction, and so on. The gA monomer can no longer extend its interaction beyond the lipid on the right side of the downward pointing arrow where the bilayer regains the form of its unperturbed thickness. Here, we have shown only they are mainly because most probably they are mainly responsible for the effective localized charges in lipids

where the Lennard–Jones potential between the two gramicidin A monomers is given by

$$U_{\mathrm{LJ}}(r) \cong U_{\mathrm{LJ}}(r^*) + \frac{1}{2}\left(\frac{\partial^2 U}{\partial r^2}\right)_{r=r^*}(r-r^*)^2 \frac{1}{6}\left(\frac{\partial^3 U}{\partial r^3}\right)_{r=r^*}(r-r^*)^3$$

$$+ \frac{1}{24}\left(\frac{\partial^4 U}{\partial r^4}\right)_{r=r^*}(r-r^*)^4 + \ldots \tag{5.17}$$

$$U_{\mathrm{LJ}}(r^*) + A'(r-r^*)^2 + B'(r-r^*)^3 + C'(r-r^*)^4 + \ldots,$$

where $r^* \approx$ average length of a hydrogen bond.

The Coulomb interaction between the two gramicidin A monomers is given by

$$U_{\mathrm{coulomb}}(r) = \frac{q_{\mathrm{gA}}^2}{4\pi\epsilon_0\epsilon_r r}. \tag{5.18}$$

The formation of a gramicidin A channel due to dimerization of two monomers inside lipid membranes is a well-studied issue. The way in which the presence of the ordered matrix of a lipid bilayer ensures the membrane-associated gramicidin A structure was already thoroughly addressed in an investigation some three decades ago [89]. The strong binding involving two gramicidin A monomers with identical charges is supported by an earlier work on the derivation of an effective attractive interaction potential between charges of the same type in solution [32]. In this chapter, the primary goal is to investigate the effect of hydrophobic bilayer thickness channel length mismatch on the stability of the already formed gramicidin A

channels. The binding energy between monomers in a channel mentioned above (Eq. 5.16) is always a standard condition, no matter how we derive this energy, and the monomer-monomer binding is kept constant throughout this study by not disturbing the membrane's inner region where the binding occurs. In the presence of a hydrophobic bilayer thickness gramicidin A channel length mismatch, τ observed in other studies was mainly seen not to follow the modest change in $U_{\mathrm{gA,gA}}$ due to a slight change of the gramicidin A monomer's charge profile in the case of binding of amphiphiles, anti-fusion, or antimicrobial peptides with channels in a varied membrane environment. All these observations, taken together, suggest that a change of (the already formed) gramicidin A channel stability is mainly due to the change of the gramicidin A channel bilayer coupling energy ($U_{\mathrm{gA,bilayer}}$), though the total potential energy between two gramicidin A monomers in a membrane-associated gramicidin A channel is given by

$$U(r) = U_{\mathrm{gA,gA}}(r) + 2U_{\mathrm{gA,bilayer}}(r). \tag{5.19}$$

Here, $U_{\mathrm{gA,bilayer}}(r)$ is the first-, second-, etc. order term in the expansion of $V_{\mathrm{sc}}(r)$ (Eqs. 5.14 and 5.15) for the hydrophobic mismatch to be filled by single, double etc. lipids representing the first-, second-, etc. order screening in the screened Coulomb interaction. The protein-protein interaction energy $\Delta G^0_{\mathrm{prot}}$, and the bilayer deformation energy $\Delta G^0_{\mathrm{def}}$ (mentioned in an earlier section) are proportional to $U_{\mathrm{gA,gA}}$ and $U_{\mathrm{gA,bilayer}}$ (in Eq. 5.19), respectively. The zeroth-order term in the expansion of $V_{\mathrm{sc}}(r)$ (Eqs. 5.14 and 5.15) represents the direct Coulomb interaction when the gramicidin A channel length exactly matches the bilayer thickness. In practice, gramicidin A channels appear with some level of hydrophobic mismatch between the bilayer thickness and the gramicidin A channel length, so there is some amount of screened Coulomb interaction to be expected. The coefficients in the interaction terms can be calculated using an energy minimum criterion $\partial U(r)/\partial r = 0$ resulting in the condition

$$A' = 2r^{*2}C'\frac{3 - r^*}{r^* - r_0}, \quad B' = 4r^*C', \tag{5.20}$$

where $r_0 (\approx (d_0 - l)/2)$ represents one-half of the hydrophobic mismatch of the bilayer thickness and the channel length.

According to Eqs. 5.14–5.19 and the description here, changes in F_{dis} (recall the definition from Eq. 5.8) could arise largely from changes in bilayer thickness (determined mainly by lipid acyl chain lengths), from changes in lipid geometry (mainly lipid curvature), changes in relative charges between lipids and gramicidin A monomers, bilayer dielectric condition, and the bilayer elastic moduli. In an experimental protocol we can vary $d_0 - l$ by choosing bilayers with different thickness or gramicidin A monomers with different lengths, or both, which consequently changes $\Delta G^0_{\mathrm{def}}$ and F_{dis} and, as a result, the stability of the gramicidin A channels becomes regulated. We discuss the experimental techniques used and a few test cases investigated in the next section. In the case when $d_0 - l \approx 0$, the channel experiences negligible destabilization due to bilayer deformation at the channel bilayer

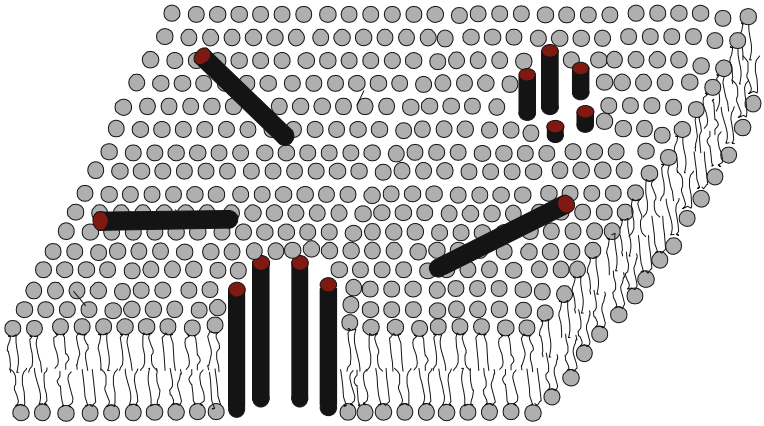

Fig. 5.8 Barrel-stave model for alamethicin channel formation inside lipid bilayers [14, 19, 36]. Cylindrical rods are schematic diagrams for alamethicin monomers in 3D view

interaction sites, but the channel may still experience slight destabilization due to any possible fluctuation in ΔG^0_{prot}.

5.2.2 Screened Coulomb Interactions and Lennard–Jones Potentials Between Peptides on Ion Channels and Lipids on the Membrane: A Study Using an Alamethicin Channel as a Tool

In the previous section, we have learned that the bilayer-spanning gramicidin A channels are formed by the reversible, trans-bilayer association of $\beta^{6.3}$-helical gramicidin A monomers [68]. Alamethicin channels form 'barrel-stave' type pores [14, 19, 36] where the alamethicin monomers align across the cylindrical surface of the channel with many possible conductance states, depending on the number of alamethicin monomers involved in the formation of a cylindrical channel (see the proposed alamethicin channel model in Figs. 5.8, 5.9 and 5.10).

Extrapolation of Gramicidin A Channel Energetics to the Alamethicin Channel

The form of V_{sc} (Eq. 5.14) in the case of alamethicin channels is still the same, but instead of considering only two screened Coulomb interactions between the channel and the bilayer at the two longitudinal ends of the channel as is considered in the gramicidin A channel's interaction sites with the bilayer, each alamethicin monomer

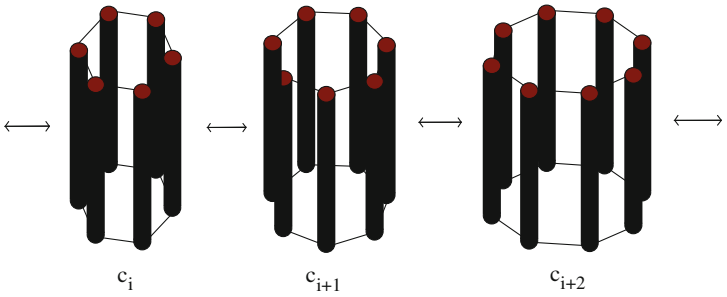

Fig. 5.9 The transition between different conduction pores of alamethicin channels

accounts for two such screened Coulomb interactions (see Eq. 5.14). The interaction between alamethicin monomers takes the form of the standard Coulomb energy formula given below:

$$U_{\text{coulomb}}(r) = \frac{1}{2}\sum_{i\neq j}^{n} \frac{q_i q_j}{4\pi\epsilon_0\epsilon_r|\boldsymbol{r_i} - \boldsymbol{r_j}|}. \tag{5.21}$$

If, for example, three monomers make the lowest conductance state in an alamethicin channel, we can assume that $|\boldsymbol{r_i} - \boldsymbol{r_j}| \approx r$. In the case of isotropic alamethicin peptides, we can also assume that $q_i q_j \approx q_{\text{Alm}}^2$ where q_{Alm} is the charge on an alamethicin monomer. However, for other higher conductance states, where the number of monomers involved is more than three, the distances between non-adjacent monomers on each cylindrical alamethicin channel should be greater than those between adjacent monomers. The term $U_{\text{LJ}}(r)$ in alamethicin channels follows an identical form to that in Eq. 5.17.

5.3 Channel Energetics and Related Probabilities in the Context of Channel Stability in Lipid Bilayers

We have discussed how we can generally apply the screened Coulomb interaction model calculation for both gramicidin A and alamethicin channels. This qualifies the model for general applications, which could involve the bilayer regulation of the functions of membrane proteins with varied structures. Despite all indications of the existence of identical bilayer membrane protein coupling energetics, the probabilities emerging from different channel conformations require an independent treatment. The gramicidin A channel's stability appears through its lifetime, which follows Eq. 5.13. That means the gramicidin A channel lifetime directly corresponds to the strength of the bilayer channel energetic coupling. This concept is also partially valid in the case of alamethicin channels and similar ones. As explained earlier,

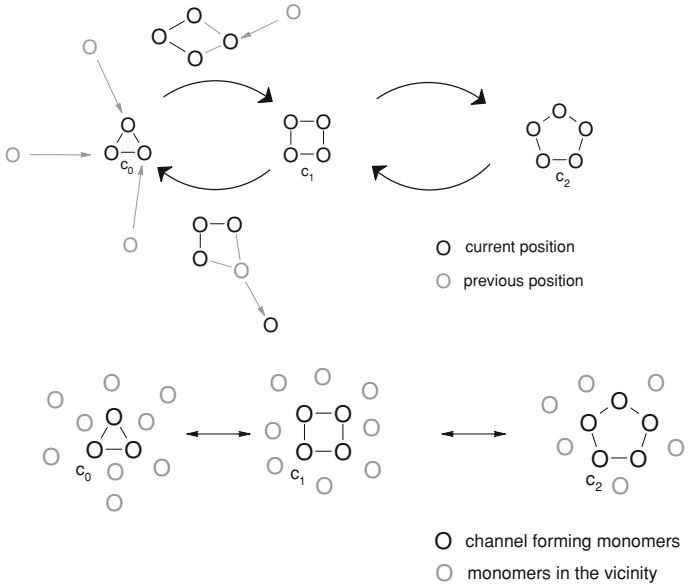

Fig. 5.10 2D view of the channels only, from the membrane surface (where alamethicin monomers are seen only along their longitudinal direction so they appear as circles) represent the two possible mechanisms of inter-channel conduction level transformations. In the bottom panel, we assume that the monomers already exist in a structured form of the alamethicin channel where the pore radius changes by reorganization of the channel forming monomers. The other 2D view illustrates a possible model of alamethicin channel formation, and a transformation between different conduction levels where the pore radius increases by addition of monomers from the surrounding space where monomers randomly move into the channel. The reduction in the pore radius occurs by releasing the monomers from the cylindrical surface of the channels. Both of the models in 2D views are valid explanations of the upper 3D structures of alamethicin channels (Figures 5.8 and 5.9). Taking three monomers in the zeroth conductance level is an arbitrary choice but the reverse calculation using experimental values of cylindrical alamethicin pore conductances and the theoretical values of the cross-sectional areas of different alamethicin pores hint that three monomers may form the zeroth conductance level. *Faded circles* and bonds in 2D views are shown to distinguish their inactivity in the channel's conduction mechanism

gramicidin A channels experience only monomer state ↔ dimer state transitions, so the channel functions do not require overly complicated analyses, but mainly the understanding of the channel stability. We have addressed this sufficiently so far for the two distinguishable gramicidin A energy states corresponding to the dimer and monomer states. However, if gramicidin A states present a continuum distribution of local energy traps, the gramicidin A channel's phenomena require a unique theoretical treatment. We briefly address this here. Due to structural complexity, alamethicin channels, and some other complex channels require complicated phenomenological models to completely explain the channel energetics. Specifically, the transitions between different channel conformations and associated independent and transition probabilities need to be clearly understood. Alamethicin channels'

independent probability corresponding to a specific energy state and transition probability between different energy states follow a straight-forward statistical mechanical formalism but a feasible physical analysis of the problem has just been published ([11] in Chap. 4). We wish to address that here first.

5.3.1 Analysis of the Alamethicin Channel Experiments

It is generally known that alamethicin channels may exist with different current levels, due to the varied number of participating alamethicin monomers. The current flowing through an alamethicin channel is directly proportional to the cross-sectional area of the cylindrical structure representing the channel. The model diagrams presented in Figs. 5.8, 5.9, 5.10 clearly address this possibility. It is also possible that any channel undergoes transitions between different structures and consequently the current through that channel undergoes transitions between different current levels. The current trace across a membrane doped with alamethicin channels shows all these features. Fig. 5.11 shows such a membrane current due to the presence of alamethicin channels inside the membrane. Detailed experimental techniques will be discussed in the next section and can be found in the literature [12].

We need to develop a unique phenomenological treatment to understand the various current transitions through alamethicin channels, as shown in Fig. 5.11 [12]. This is done below.

The probability (W_i) of an alamethicin channel having a current level i is estimated as:

$$W_i = \frac{A_i}{\sum_{i=0}^{n} A_i + A_{\mathrm{nc}}}, \tag{5.22}$$

where A_i denotes the area under the peak in the current level histogram (see Fig. 5.11c) representing a current level i ($i = 0, 1, 2, 3, \ldots, n$, where $n + 1$ is the maximal number of current levels in the experiment) and A_{nc} is the area under the peak representing the baseline (no channels). The probability of the channel having a current level i, relative to the baseline, is given by

$$r_i = \frac{A_i}{A_{\mathrm{nc}}} = \frac{W_i}{W_{\mathrm{nc}}} = \exp\left(-\frac{\Delta G^{\mathrm{nc}\to i}}{k_B T}\right), \tag{5.23}$$

where $\Delta G^{\mathrm{nc}\to i}$ (which still needs to be normalized by the alamethicin monomer concentration in the bilayer) is the free energy of the channel in current level i relative to the baseline, T is the temperature in kelvin, and k_B is Boltzmann's constant. $\Delta G^{\mathrm{nc}\to i}$ is, in fact, a measure of the change in the bilayer deformation energy required to form an alamethicin channel in a bilayer membrane.

It turns out to be helpful to consider the probability of having a current level, relative to the baseline

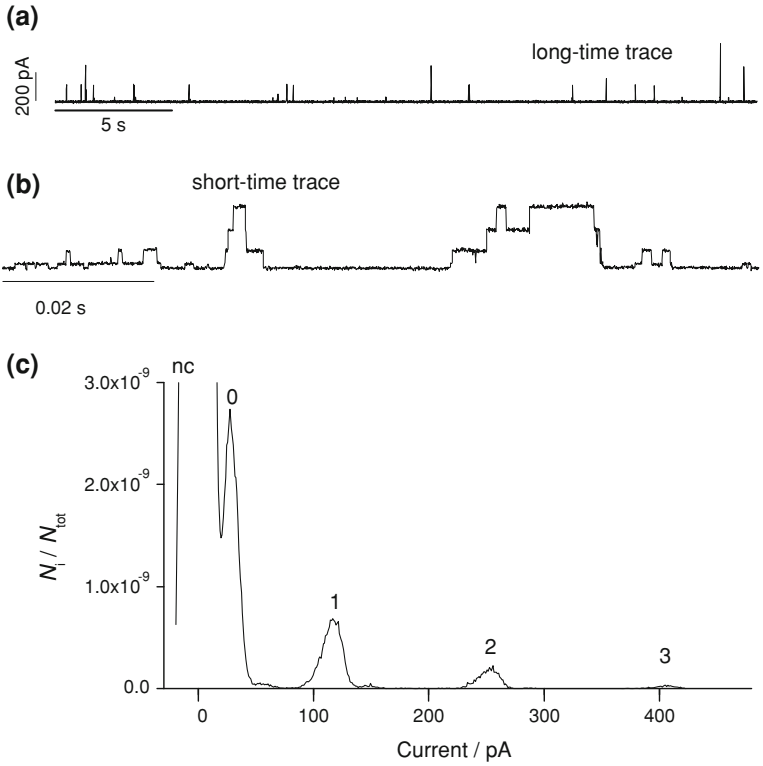

Fig. 5.11 Alamethicin channel activity in a 1,2-Dioleoyl-sn-Glycero-3-Phosphocholine ($DC_{18:1}PC$)/n-decane bilayer. **a** and **b**, long- (30 s) and short- (0.1 s) time records, respectively, of current traces through alamethicin channels. **c** current level histograms obtained from 30 s traces. N_i is the point count at any value of current ($\geq$ 0pA) and $\sum_i N_i = N_{\text{tot}} (= 2 \times 10^6)$ is the total point count during the whole record time. Sum of the probabilities ($W_{\text{nc}} + W_0 + W_1 + W_2 + W_3 + \ldots$) is 1.0 ($W_i = N_i/N_{\text{tot}}$) in the point count plots. W_{nc}, W_0, W_1, W_2, W_3, etc. are 9809.19×10^{-4}, 134.43×10^{-4}, 42.305×10^{-4}, 12.39×10^{-4}, 1.68×10^{-4}, etc. respectively. Current levels 0, 1, 2, and 3 are at 29 ± 2, 113 ± 5, 243 ± 9, and 386 ± 10pA, respectively. Mean $\pm$ S.D., $n \geq 6$ are the numbers of current traces collected at independent experimental conditions. Trans-membrane applied potential V = 150 mV. Alamethicin was added to the trans side of the lipid bilayer at $\sim 10^{-8}$ molar (M) in the aqueous phase bathing the lipid bilayer. The cis side was the electrical ground. The aqueous phase contained 1.0 M NaCl, pH 7.0

$$r_{\text{tot}} = \sum_{i=0}^{n} r_i \tag{5.24}$$

such that the changes of the properties of an alamethicin channel hosting a lipid bilayer, such as thickness, lipid curvature, bilayer elasticity, etc. alter the value of r_{tot}, but the value can be kept constant or at least comparable by changing the alamethicin channel molar concentration in the aqueous phase. However, the

relative probabilities of observing different current levels (channel conformations) e.g., W_{j+k}/W_j between levels $j+k$ and j, may show different control values as the bilayer properties change. The corresponding free energy distribution between different current levels can be determined by

$$\frac{W_{j+k}}{W_j} = \exp\left(-\frac{\Delta G^{j\to j+k}}{k_B T}\right), \tag{5.25}$$

where $\Delta G^{j\to j+k}$ is the free energy of the channel in current level $j+k$ relative to level j.

5.3.2 Derivation of Gramicidin A Channel Lifetime (τ) in a Continuum Distribution of Local Energy Traps

As discussed earlier, the relationship between the lifetime and the deformation energy change is proposed to be: $\tau = \exp(-\frac{\Delta\Delta G^{\ddagger}_{\text{def}}}{k_B T})$ (Eq. 5.13) which assumes that the difference in protein transition energy $\Delta\Delta G^{\ddagger}_{\text{prot}}$ does not change considerably as the gramicidin A subunits move apart by a distance $(\lambda^+ - \lambda)$ to dissociate from each other [30]. For a particular bilayer deformation, the negative exponential energy dependence of the channel lifetime is a valid approximation. However, in the case where a continuum distribution of local energy traps is involved, an integration over all trap levels is needed to find the average value of the channel lifetime τ_{av}. Here, the appropriate formula to be used is

$$\tau_{\text{av}} = \int \tau \exp\left(-\frac{\Delta E}{k_B T}\right)\rho(E)\mathrm{d}E, \tag{5.26}$$

where ΔE stands for $\Delta\Delta G^{\ddagger}_{\text{def}}$ (for simplicity) and $\rho(E)$ denotes the probability distribution of having a trap with a particular energy level. Following the detailed calculations provided in reference [85] we find that the dependence of the average lifetime τ_{av} on deformation energy change $\Delta\Delta G^{\ddagger}_{\text{def}}$ transforms from exponential to a power law relation:

$$\tau_{\text{av}} \approx (\Delta\Delta G^{\ddagger}_{\text{def}})^{-a} \approx ((\lambda^+ - \lambda)F_{\text{dis}})^{-a}. \tag{5.27}$$

Here, a is a parameter which is dependent on chemical and thermodynamic conditions.

5.4 Experimental Studies of the Functions of Gramicidin A and Alamethicin Channels in Lipid Membranes

So far we have discussed theoretical aspects of both gramicidin A and alamethicin channel functions in lipid membranes. We have successfully addressed how membrane protein functions become regulated due to energetic lipid bilayer membrane protein coupling, using a very traditional theoretical approach which involves screened Coulomb interactions [9]. Although both of these channels have been extensively experimentally investigated, we reiterate some of the aspects of the experimental studies using our own investigations (see [11] in Chap. 4). The rather novel parameters emerging from the studies help to validate the theoretical approaches explained in earlier sections. These experimental studies were done by Md Ashrafuzzaman in collaboration with Dr. Olaf Sparre Andersen during his tenure in Cornell University Weill Medical College.

5.4.1 Materials and Methods

Materials

1,2-Dioleoyl-sn-Glycero-3-Phosphocholine ($DC_{18:1}PC$), 1,2-Diecosenoyl-sn-Glycero-3-Phosphocholine ($DC_{20:1}PC$), 1,2-Dierucoyl-sn-Glycero-3-Phosphocholine ($DC_{22:1}PC$), 1,2-dioleoyl-sn-glycero-3-phosphoethanol-amine ($DOPE$), and 1,2-dioleoyl-sn-glycero-3-[phospho-L-serine] ($DOPS$) were from Avanti Polar Lipid (Alabaster, AL, USA) and used without further purification. *n*-Decane was 99.9 % pure from ChemSampCo (Trenton, NJ, USA) and squalene (squalene was filtered through chromatographic alumina (acid type) from Sigma to make it radical-free) was from Sigma (St. Louis, MO, USA). Alamethicin (Alm), an antibiotic from Tricoderma viride that is a mixture of alamethicin homologs, was from Sigma. Gramicidin A (gA) analogue [Ala^1]gA (with 15 amino acids in the sequence) (AgA(15)) and the sequence-shortened analogue, des-(D − Val^1 − Gly^2)-gA (with 13 amino acids in the sequence) ($gA^-(13)$) were generous gifts from Drs. R.E. Koeppe II and D.V. Greathouse (see [11] in Chap. 4). They were synthesized and purified as described in [31]. The amino acid sequences, channel lengths, phospholipids, bilayer thicknesses and abbreviations used in this article are shown in Tables 5.1 and 5.2. The electrolyte solution (NaCl) was buffered with N-2-Hydroxyethylpiperazine-N'-2-ethanesulfonic Acid (HEPES) (pH 7.0) and was from Sigma.

Methods

Planar lipid bilayers were formed from $DC_{18:1}PC$, $DC_{20:1}PC$, $DC_{22:1}PC$, $DOPE$ or $DOPS$/*n*-decane or squalene (2.5 % w/v) solutions across a 1.5 mm hole in

Table 5.1 Gramicidin sequences and their channel lengths

Gramicidin analogue	Abbreviation	Sequence	Hydrophobic Channel Length [41] Å
[Ala^1]gA	AgA(15)	f-A-G-A-L-A-V-V-V-W-L-W-L-W-L-W-ea	22
Des-(D-Val^1-Gly^2)gA	$gA^-(13)$	f-A-L-A-V-V-V-W-L-W-L-W-L-W-ea	19

Table 5.2 Phospholipids and their thicknesses

Phospholipid	Abbreviation	Bilayer Thickness (with *n*-decane) Å
1,2-dioleoyl-*sn*-glycero-3-phosphocholine	$DC_{18:1}PC$	47.7 ± 2.3 [16]
1,2-diecosenoyl-*sn*-glycero-3-phosphocholine	$DC_{20:1}PC$	53.9 ± 2.5 [16]
1,2-dierucoyl-*sn*-glycero-3-phosphocholine	$DC_{22:1}PC$	58.4 ± 2.5 [16]
1,2-dioleoyl-*sn*-glycero-3-phosphoethanolamine	$DOPE$	Unknown
1,2-dioleoyl-*sn*-glycero-3-phospho-L-serine	$DOPS$	Unknown

Teflon® separating the two electrolyte solutions of 2.5 mL each, using the pipette method of Szabo et al. [83]. All experiments were performed at 25 ± 0.5 C. The aqueous electrolyte solutions were 1.0 M NaCl, buffered to pH 7.0 using 10 mM HEPES added to the solution. Care was taken to minimize the total amount of lipid (and *n*-decane or squalene) that was added; the total volume of the lipid/decane or squalene solution was typically 1,000-times smaller than the volume of the aqueous solution.

For the experiments with Alm, we added an appropriate amount of Alm from its 10^{-5} M stock solution in dimethyl sulfoxide to the *trans* side of the lipid bilayer; the *cis* side was the electrical ground. In the experiments across DOPE and across thicker bilayers of $DC_{20:1}PC$ and $DC_{22:1}PC$, we needed a 10-fold and more than 10–100-fold denser solution of Alm compared to that for $DC_{18:1}PC$. Experiments with gA were done in $DC_{18:1}PC$/*n*-decane or squalene, $DC_{20:1}PC$/squalene and $DOPE$/*n*-decane bilayers with a 15-residue and a 13-residue gA analog of opposite chirality, e.g. AgA(15) and $gA^-(13)$ (added to both sides of the bilayer), an experimental design that allows for a direct test of how changes in the hydrophobic mismatch due to changes in the channel length may affect the channel stability. The reason for using gA analogs of opposite chirality is to ensure against the formation of heterodimers between the 13-amino acid and 15-amino acid analogs [25, 50] which would complicate the data analysis. Using lipids with different acyl chain lengths results in changing the bilayer thickness, and also in the hydrophobic mismatch between bilayer thickness and channel lengths (see Tables 5.1 and 5.2). In all experiments with Alm channels, the applied potential across the membrane was 150 mV, and with gA analogs the applied potential was 200 mV.

After peptide addition, the aqueous phases were stirred for about 5 min before the measurements resumed. The total amount of added dimethyl sulfoxide was less than 0.5 % of the volume of the electrolyte solution, a concentration that has no effect on Alm or gA channel function. The lipid bilayer membrane containing *n*-decane was 3–4 h stable whereas the membrane containing squalene was very unstable, especially when a potential was applied across the membrane.

Single-channel experiments were performed using the bilayer-punch method [4] and a Dagan 3900A patch-clamp amplifier (Dagan Corp., Minneapolis, MN) with a 3910 bilayer-expander module. The current signal in experiments with Alm channels was filtered at 20 kHz, and digitally filtered at 8 kHz while the current signal in experiments with gA channels was filtered at 2 kHz, digitized at 20 kHz, and digitally filtered at 500 Hz before the single-channel transitions were detected using the algorithm described by Andersen [4] and implemented in Visual Basic (Microsoft Corp., Redmond, WA). Relative total times spent by different open (conducting) states and the closed (non-conducting) state of Alm channels were determined by using frequency counts (in Origin 6.1 from OriginLab Corp., Northampton, MA) of the recorded current traces of about 1–3 min. The frequency counts were plotted as functions of the conductance of Alm channels for each recorded current trace, and peaks were found at the non-conducting and all conducting levels.

Single-channel lifetimes for gA channels were determined as described by Sawyer et al. [78] and Durkin et al. [25], a procedure that allows for separate determination of the lifetimes of different channel types.

5.4.2 Results

Gramicidin A Channel Results

Figure 5.12a shows representative current traces obtained in the $DC_{18:1}PC/n$-decane bilayer in the presence of gA^- (13) and AgA(15). Figure 5.12b shows how gA channels formed from different gA monomers appear with different current transition amplitudes, namely gA^- (13) channels at 1.95 ± 0.12 pA and AgA(15) channels at 3.05 ± 0.11 pA, respectively. The average gA channel lifetimes (τ) were estimated by fitting a single-exponential distribution (see Fig. 5.12c)

$$\frac{N(t)}{N(0)} = \exp\left(\frac{t}{\tau}\right), \tag{5.28}$$

where $N(t)$ is the number of channels lasting longer than time t (for details see [13]).

Figure 5.13 summarizes the average lifetimes $\tau_{\mathrm{AgA(15)}}$ and $\tau_{\mathrm{gA^-(13)}}$ of gA channels formed by dimerization of two gA monomers AgA(15) and gA^-(13), respectively, in lipid bilayers of different thickness (see Table 5.2). In a $DC_{18:1}PC$ bilayer we observe that by increasing the gA channel length by only about 3 Å

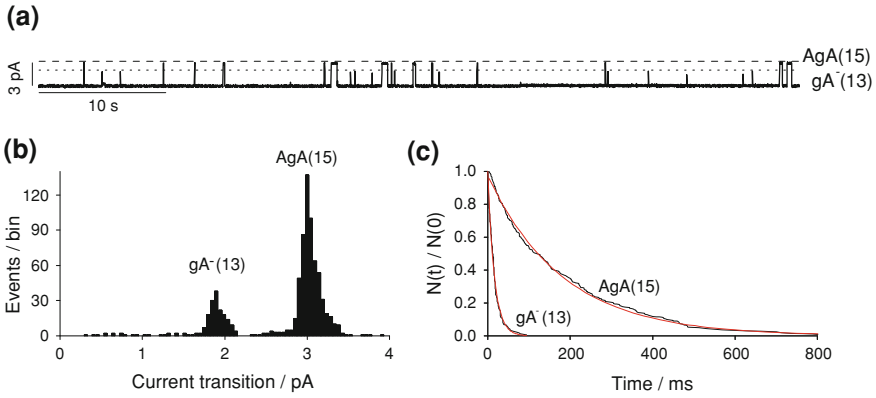

Fig. 5.12 **a** A 60 s current traces recorded from a $DC_{18:1}PC/n$-decane bilayer that was doped with gA^- (13) and AgA(15) on both sides. **b** The current transition amplitudes for gA^-(13) and AgA(15) channels are 1.95 ± 0.12 and 3.05 ± 0.11 pA. **c** Lifetime histograms (and their exponential fits) for gA^-(13) channels and AgA(15) channels (for details see [13])

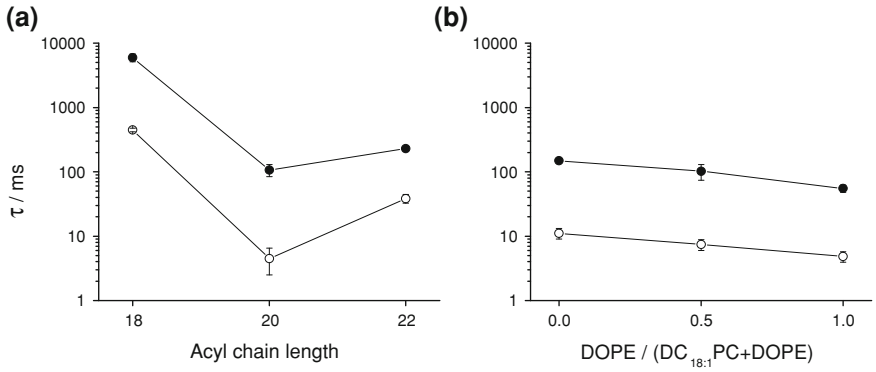

Fig. 5.13 Average τ (gA dimers of AgA(15) or gA-(13)) changes with d_0 (A. squalene in bilayer reduces d_0 over n-decane, τ increases 35-fold) and c_0 (B. introducing 1,2-dioleoyl-*sn*-Glycero-3-phosphoethanolamine (DEPE) into membranes/n-decane). For experimental protocols and methods see [13]. Acyl chain lengths 18, 20, and 22 represent bilayer-constructing lipids $DC_{18:1}PC$, $DC_{20:1}PC$, and $DC_{22:1}PC$, respectively. Trans-membrane potential 200 mV. Aqueous conditions 1.0 M NaCl, pH 7.0 (see [11] in Chap. 4)

the channel stability increases approximately 13-fold ($\tau_{\mathrm{AgA(15)}} = 149 \pm 11$ ms and $\tau_{\mathrm{gA^-(13)}} = 11.2 \pm 2.1$ ms, consequently the ratio $\tau_{\mathrm{AgA(15)}}/\tau_{\mathrm{gA^-(13)}} \approx 13$). Under identical conditions, if we replace the PC bilayer by a more negative curvature bearing DOPE bilayer [49] with comparable thickness [52], we observe that both short ($gA^-(13)$) and long ($AgA(15)$) gA channels experience almost equal (~2.5-fold) destabilization (see Fig. 5.13). Here, by using a shorter $gA^-(13)$ monomer over a longer $AgA(15)$ monomer we have introduced a higher (~3 Å) hydrophobic mismatch between the bilayer thickness and the channel length. As a consequence,

we have observed a 13-fold reduction in the gA channel lifetime. Whereas by replacing $DC_{18:1}PC$ bilayer with DOPE bilayer bearing a relatively more negative curvature with comparable thickness [52] we observe much less reduction in the gA channel lifetime for both short and long gA channels, and the stepwise introduction of DOPE (0, 50, and 100 %) over $DC_{18:1}PC$ we observe that the gA channel lifetime decreases almost linearly with an increasing negative curvature (see Fig. 5.13). This observation suggests that bilayer thickness and the gA channel length mismatch appears as a stronger gA channel regulator than the lipid curvature. On the other hand, we observe that the shorter gA channels are about 13- and 23-fold less stable than longer gA channels in $DC_{18:1}PC$/squalene (thinner bilayer) and $DC_{20:1}PC$/squalene (thicker bilayer) bilayers, respectively. We also observe that shorter $gA^-(13)$ and longer $AgA(15)$ channels become about 100- and 55-fold less stable, respectively, when equal amounts of increase in the hydrophobic mismatch between bilayer thickness and gA channel lengths for both $gA^-(13)$ and $AgA(15)$ channels occur by replacing $DC_{18:1}PC$ with $DC_{20:1}PC$ in squalene-containing lipid bilayers. With a further increase in bilayer thickness, by choosing $DC_{22:1}PC$ lipids to form lipid bilayers, we observe no formation of linear β-helical gA dimers, probably due to extremely high values of the hydrophobic bilayer thickness gA channel length mismatch $(d_0 - l)$. Nonetheless, even under this condition the gA channels are still formed, although a different conformational mechanism is at work, namely the gA monomers no longer form linear dimers as shown in the model diagram (see Fig. 5.2) but instead the monomers partially bind with each other through their whole lengths [62]. Thus, the channel length is on the order of just a single gA monomer and not on the order of the sum of two gA monomer lengths (see Fig. 5.2). These experimental results, taken together, suggest that the increase in hydrophobic mismatch between bilayer thickness and the gA channel length by either increasing the lipid acyl chain length or reducing the gA channel length appears as a very strong regulator of gA channel stability. Lipid curvature is also an important regulator of gA channel stability, but not as strong as $(d_0 - l)$. Another important parameter is the peptide concentration required to form readily observable gA channels in lipid bilayers. The appearance frequency of gA channels f_{gA} increases more rapidly (proportional to the second power or greater) than the gA monomer concentration ($[M_{gA}]$), although the average gA channel lifetime remains almost unchanged. The required peptide concentration is therefore an important parameter in determining the change of bilayer deformation energy. We observe that about a 100-fold higher $[M_{gA}]$ is required in the $DC_{20:1}PC$ bilayer over the $DC_{18:1}PC$ bilayer while about a 10-fold higher $[M_{gA}]$ is required in the DOPE bilayer over the $DC_{18:1}PC$ bilayer. Here, we also observe higher effects on the gA channel appearance frequency f_{gA} due to the change of $d_0 - l$ than those due to the lipid intrinsic curvature.

Alamethicin Channel Results

We have already presented a representative current trace obtained in the $DC_{18:1}PC$/*n*-decane bilayer in the presence of Alm peptide in Fig. 5.11. To initiate the formation

of considerable Alm channel activity under the experimental conditions, a minimum of 10^{-8} M Alm peptide concentration ($[M_{\mathrm{Alm}}]$) is required in $DC_{18:1}PC/n$-decane bilayers [12]. However, once the Alm channel starts showing, we observe that the Alm channel activity increases considerably (reported in earlier observations to be a power of 2.6 of the concentration at 25 °C [51]) as $[M_{\mathrm{Alm}}]$ increases. We also observed that the Alm channel activity shows significant dependence on bilayer thickness and on lipid curvature. Higher lipid charges also considerably destabilize the probability of observing any Alm channel current level, especially higher order current levels [18]. To observe comparable Alm channel activity (i.e., comparable value of $\sum_i r_i = \sum_i (A_i/A_{\mathrm{nc}})$ (see Sect. 5.3.1), where A_i and A_{nc} are the areas under the peaks representing a current level i and the baseline in Alm channel current traces as shown in Fig. 5.11), about 10^{-8} M of $[M_{\mathrm{Alm}}]$ in $DC_{18:1}PC/n$-decane bilayers was required while 10-fold higher ($\sim 10^{-7}$ M) of $[M_{\mathrm{Alm}}]$ was required in DOPE/n-decane (also previously observed (see [11] in Chap. 4)) or DOPS/n-decane bilayers (with a very low probability of observing higher order current levels in bilayers formed with DOPS lipids). On the other hand, a more than 10- or even 100-fold increase in the concentration $[M_{\mathrm{Alm}}]$ was required when $DC_{18:1}PC$ was replaced with $DC_{20:1}PC$ or $DC_{22:1}PC$ bilayers containing n-decane or squalene to observe comparable Alm channel activity. The additional free energy ($\Delta G^{\mathrm{nc}\to i} = -k_B T \ln r_i$) (see earlier section) involved in raising any current level in an Alm channel in thicker bilayers or bilayers with higher amounts of negative curvature is perhaps compensated by the requirement of a higher $[M_{\mathrm{Alm}}]$ [92]. Once comparable Alm channel activity is observed, the relative probability of observing different Alm conductance levels e.g., $j+k$ and jW_{j+k}/W_j (see Sect. 5.3.1) in different bilayer system is also found to be different, but does not vary within the same lipid system. The values of W_2/W_1 and W_3/W_1 are observed to be 0.25 ± 0.05 and 0.04 ± 0.01 for $DC_{18:1}PC$, 1.38 ± 0.21 and 0.88 ± 0.21 for $DC_{20:1}PC$, 1.52 ± 0.2 and 1.06 ± 0.25 for $DC_{22:1}PC$, and 2.05 ± 0.8 and 2.23 ± 1.0 for DOPE/n-decane bilayers. Consequently, the mean values of the changes in average free energies $\Delta G^{1\to 2}$ and $\Delta G^{1\to 3}$ are observed to be $-0.6 k_B T$ and $-1.39 k_B T$ for $DC_{18:1}PC$, $0.14 k_B T$ and $-0.55 k_B T$ for $DC_{20:1}PC$, $0.182 k_B T$ and $0.025 k_B T$ for $DC_{22:1}PC$, and $0.31 k_B T$ and $0.35 k_B T$ for DOPE/n-decane bilayers. The values of W_2/W_1 and W_3/W_1 are observed to be 0.21 ± 0.15 and 0.053 ± 0.04, respectively. Consequently, $\Delta G^{1\to 2}$ and $\Delta G^{1\to 3}$ are found to be $-0.68 k_B T$ and $-1.28 k_B T$, respectively, in DOPS/n-decane bilayers with negligible presence of current levels above the third current level.

5.5 Theoretical Results/Numerical Results Regarding the Functions of Gramicidin A and Alamethicin Channels Due to Their Coupling with Lipid Membranes

Based on the model of gA channels in lipid bilayers (see Fig. 5.2) we deduce that any gA channel exists in a lipid bilayer through bilayer deformations at the channel bilayer interfaces to compensate for the hydrophobic mismatch ($d_0 - l$) between

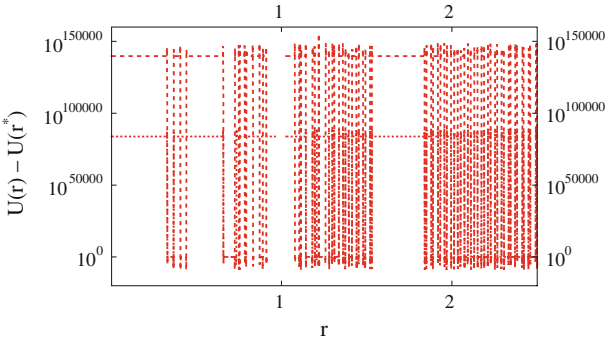

Fig. 5.14 Plot of the energy as a function of the reaction coordinate (using Eq. 5.19 here and hereafter) for gA channels in lipid bilayer energetics at different orders of screening (single- and double-dashed curves are for the first- and second-order screening, respectively). Only real parts of the energies have been considered and for simplicity $U(r*)$ has been used for $U_{\rm LJ}(r*)$ here and other energy plots in all next figures. $q_L/q_{\rm gA} = 0.005$, $(1/\epsilon_0)q_L q_{\rm gA} \approx 1$ has been chosen (here and in Figs. 5.15 and 5.16) for simplicity, $r_{\rm LL} = 7.74597$ Å. In the plot, the energy at $r = 0$ Å has been excluded to avoid the associated singularity. Numerical integration here (and hereafter) has been performed using Mathematica 7 within $(-k_{\rm max}2\pi/r_{\rm LL}, k_{\rm max}2\pi/r_{\rm LL})$, where $k_{\rm max} = 100$ and the step size for integration $d_r = 0.001$ have been taken as judicious choices

bilayer thickness and gA channel lengths. The 'barrel-stave' pore type Alm channels (see Fig. 5.8) [19, 36] exist with different sizes, depending on the number of Alm monomers participating in the pore formation and the pore continuously experiences structural transitions between different conformations representing different pore conductance levels (which experimentally manifest themselves as current levels) following the energetic profile as described in Sect. 5.3.1. Note that the higher the cross-sectional area of the pore, the higher the value of the conductance through the Alm channel.

Figures 5.14, 5.15, and 5.16 demonstrate the energetics (in arbitrary units) of a gA channel in lipid bilayers with different lipid screening orders and lipid dimensions using the model calculation. In Figs. 5.14 and 5.15 G_I and G_{II} ($G_I > G_{II}$) represent energy levels at conformational states I and II where two gA monomers exist in free form (no channel formation: M_I) and gA dimer form (channels formed: D_{II}), respectively. Formation of a channel with any level of stability requires an energetic transition (reduction) $\Delta G_{I,II}$ $(= G_I - G_{II})$. Although the energy minima appear at different values of reaction coordinates, we have chosen the transition $G_I \leftrightarrow G_{II}$ at a certain value of reaction coordinate (as shown in Fig. 5.15) to illustrate how the corresponding back-and-forth conformational changes between gA monomers and dimers ($M_I \Leftrightarrow D_{II}$) may become regulated due to $\Delta G_{I,II}$, which depends mainly on the bilayer physical properties for a certain channel type. The binding energy between two gA monomers alone in a gA channel is many orders of magnitude smaller than the binding energy of the gA channel with the bilayer at the channel bilayer interface. $\Delta G_{I,II}$ (see Figs. 5.14 and 5.15) represents the amount of energy gA monomers need

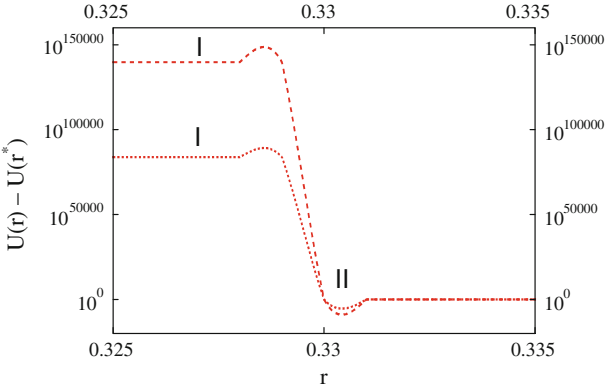

Fig. 5.15 A plot of the energy as a function of the reaction coordinate for gA channels in lipid bilayer energetics at different orders of screening (single- and double-dashed curves are for the first- and second-order screening, respectively). I and II represent levels with free energies G_I and G_{II} respectively, where gA monomers exist as free (no channel formed) and gA dimer (gA channel formed). $q_L/q_{\mathrm{gA}} = 0.005$, $r_{\mathrm{LL}} = 7.74597$ Å. *Ad hoc* assumptions ($q_{\mathrm{gA}} \sim$ electron charge and other relevant parameters [1, 16, 17, 35, 41, 71, 75]) give an estimate of G_I and G_{II} to be 10^{-1} and 10^{-8} in first-order and 10^5 and 10^{-4} in second-order lipid screening in units of kJ/mole which seriously depends on q_L as d_0 increases. The energy orders for G_I and G_{II} as mentioned here are also valid approximations for the corresponding free energy levels presented in the subsequent Figs. 5.16, 5.17, and 5.18

to compensate to form a stable gA channel which arises mainly from the hydrophobic binding between the gA channel and the bilayer at the two bilayer channel interfaces. The smaller the value of $\Delta G_{I,II}$, the higher the stability of gA channels. We observe that the value of $\Delta G_{I,II}$ for the second-order lipid-screening is orders of magnitude higher than that for the first-order lipid-screening (higher orders of lipid screening account for higher values of $d_0 - l$). Knowing the effective values of charges (in units of coulombs) on a gramicidin monomer, q_{gA}, and that of a lipid's head group region, q_L, one can readily calculate and show in real energy units (J), using the screened Coulomb interaction theory, that G_I has values which are drastically reduced and hence the value of $\Delta G_{I,II}$ collapses as the value of $d_0 - l$ approaches 0 Å. For example, making an *ad hoc* assumption that q_{gA} and q_L should be on the order of a few electron charges, we find $\Delta G_{I,II}$ to be on the order of kJ/mole for the first-order lipid screening, which closely corresponds to the phenomenological bilayer deformation energy calculated in another study [13]. The same *ad hoc* assumption ensures that $\Delta G_{I,II}$ increases to the order of 105 kJ/mole for the second-order lipid screening. This drastic increase in bilayer deformation energy requirements for stable channel formation with increasing the bilayer thickness channel length mismatch causes gA channel formation to be extremely difficult at a higher order of lipid screening. Beyond a certain level of hydrophobic bilayer channel mismatch, the deformation energy reaches values which are outside a biological binding energy scale, which suggests that at this high energy level the β-helical gA channels must experience

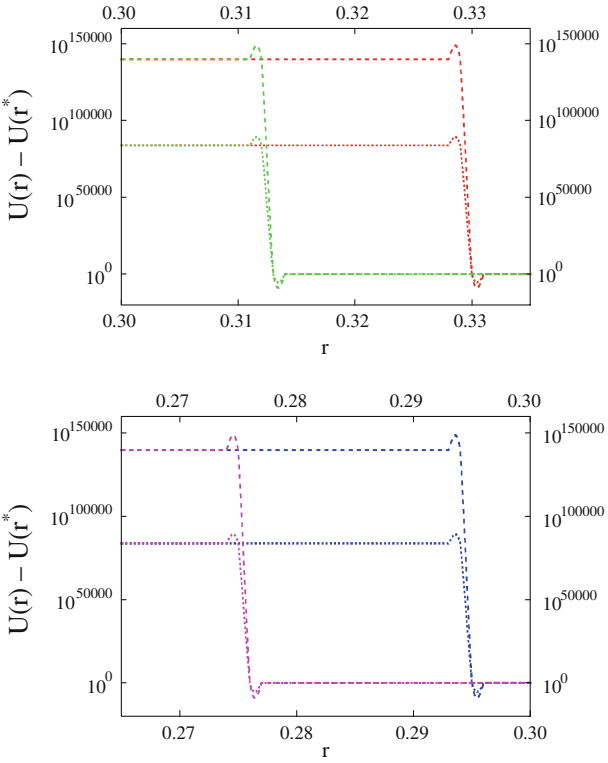

Fig. 5.16 A plot of the energy as a function of the reaction coordinate for a gA channel in lipid bilayer energetics at different values of r_{LL} (left $\rightarrow$ right: $r_{\mathrm{LL}} = 6.48074$, 6.9282 (*lower panel*), 7.34847, 7.74597 Å (*upper panel*)) for the first- (single-dashed curve) and second-(double-dashed curve) order lipid screening. $q_L/q_{\mathrm{gA}} = 0.0025$

exponential growth in their instability and finally may undergo a structural transition which has been experimentally observed (see Fig. 5.13). As $(d_0 - l)$ approaches 0 Å, the drastic drop in the values of G_I causes the value of $U(r)$ to quickly approach the level whose order of magnitude is comparable to that of the smaller interaction energy level ($U_{\mathrm{gA,gA}}(r)$—see Eq. 5.16) between two gA monomers with only direct Coulomb binding effects with the bilayer. Under this condition, the bilayer deformation energy is no longer an important regulator of channel function. Figure 5.16 demonstrates that the geometry of the lipids is an important regulator, and the transition $G_I \leftrightarrow G_{II}$ occurs at increasing reaction coordinates with increasing values of lipid dimension parameter r_{LL}. Identical trends with quantitatively slightly different energetics have been observed for Alm channels in lipid bilayers (see Figs. 5.17 and 5.18).

Figures 5.19 and 5.20 show how lipid charge relative to the charge of the channel-forming peptides changes the values of both G_I and G_{II} (see Fig. 5.19) and

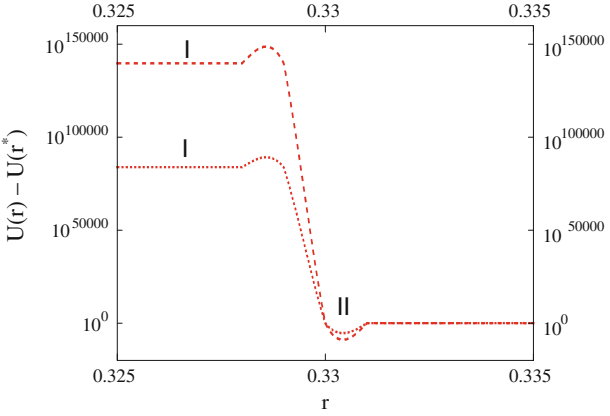

Fig. 5.17 A plot of the energy as a function of the reaction coordinate for Alm channels in lipid bilayer energetics at different order of screening (single- and double-dashed curves are for the first- and second-order screening, respectively). Here and in Fig. 5.18, $q_L/q_{\text{Alm}} = 0.005$, $(1/\epsilon_0)q_L q_{\text{Alm}} \approx 1$ has been chosen (for simplicity), and $r_{\text{LL}} = 7.74597$ Å

consequently $\Delta G_{I,II}$ (see Fig. 5.20). We observe about three times higher values of both G_I and G_{II} for both the first- and second-order of lipid screening for an Alm channel with three monomers in the 'barrel-stave' pore, compared to a gA channel as shown in Fig. 5.19. Quantitatively similar (3-fold increases) higher values of $\Delta G_{I,II}$ (see Fig. 5.20) are observed for both lipid screening orders for an Alm channel, compared to those for a gA channel. The three-times higher values of G_I, G_{II}, and $\Delta G_{I,II}$ in the Alm channel with three monomers are obvious, because in this specific Alm channel conformation there are six channel bilayer interaction sites, while a gA channel always has only two interaction sites with the bilayer (see Figs. 5.2 and 5.8). It seems that the interaction energy between monomers in both gA and Alm channels becomes irrelevant in comparison to the binding energy between the channel and the bilayer. We also observe that G_I, G_{II} and $\Delta G_{I,II}$ increase with the increase of lipid peptide charge ratio following:

$$G_I, G_I, \Delta G_{I,II} \propto \left(\frac{q_L}{q_M}\right)^3, \tag{5.29}$$

where $s = 1, 2$, etc. for the first-, second-, etc. order lipid screening, respectively, for both gA and Alm channels. Here, q_M stands for gA (q_{gA}) or Alm (q_{Alm}) monomer charges.

In Fig. 5.21 we observe a modest and linearly proportional effect of the lipid dimension r_{LL} on $\Delta G_{I,II}$, for both the first- and second-order lipid screening with three-times higher effects for Alm channels than for gA channels. Figure 5.22 shows that, for both gA and Alm channels, the reaction coordinate at which we have shown

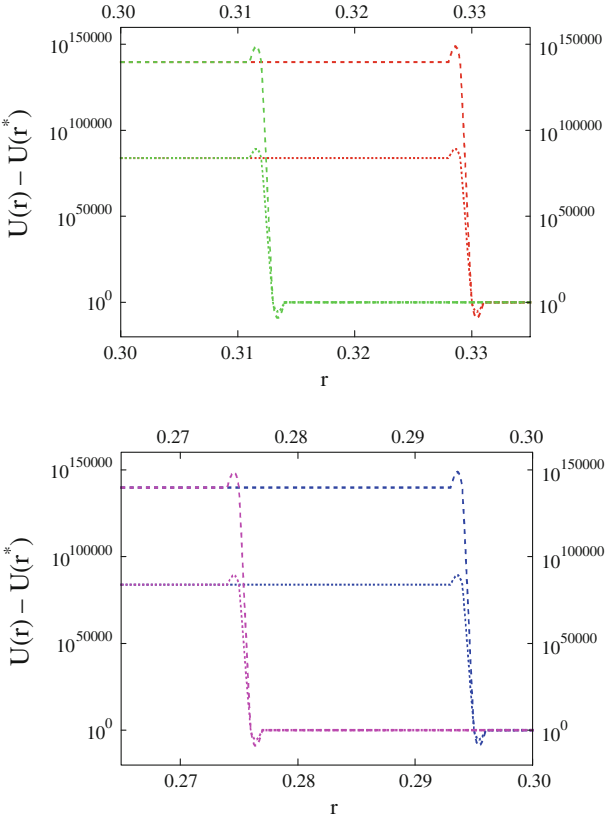

Fig. 5.18 A plot of the energy as a function of the reaction coordinate (r) for an Alm channel in lipid bilayer energetics at different values of r_{LL} (left $\rightarrow$ right: $r_{\mathrm{LL}} = 6.48074$, 6.9282 (*lower panel*), 7.34847, 7.74597 Å (*upper panel*)) for the first- (single-dashed curve) and second-(double-dashed curve) order lipid screening. $q_L/q_{\mathrm{Alm}} = 0.0025$

the calculation of $\Delta G_{I,II}$ increases (shifts toward higher values) in linear proportionality to r_{LL} for both the first- and second-order lipid screening.

The most dramatic theoretical result is illustrated in Fig. 5.23, where $\Delta G_{I,II}$ increases exponentially with the increase of $d_0 - l$ (here we have rephrased the order of screening by $d_0 - l$):

$$\Delta G_{I,II} \propto \exp(d_0 - l). \tag{5.30}$$

Consequently, as $\Delta G_{I,II}$ is proportional to $\Delta G^0_{\mathrm{def}}$, the dissociation force:

$$F_{\mathrm{dis}} = -\left(-\frac{\partial \Delta G_{I,II}(d_0 - l)}{\partial (d_0 - l)}\right) \tag{5.31}$$

also follows an exponential relation:

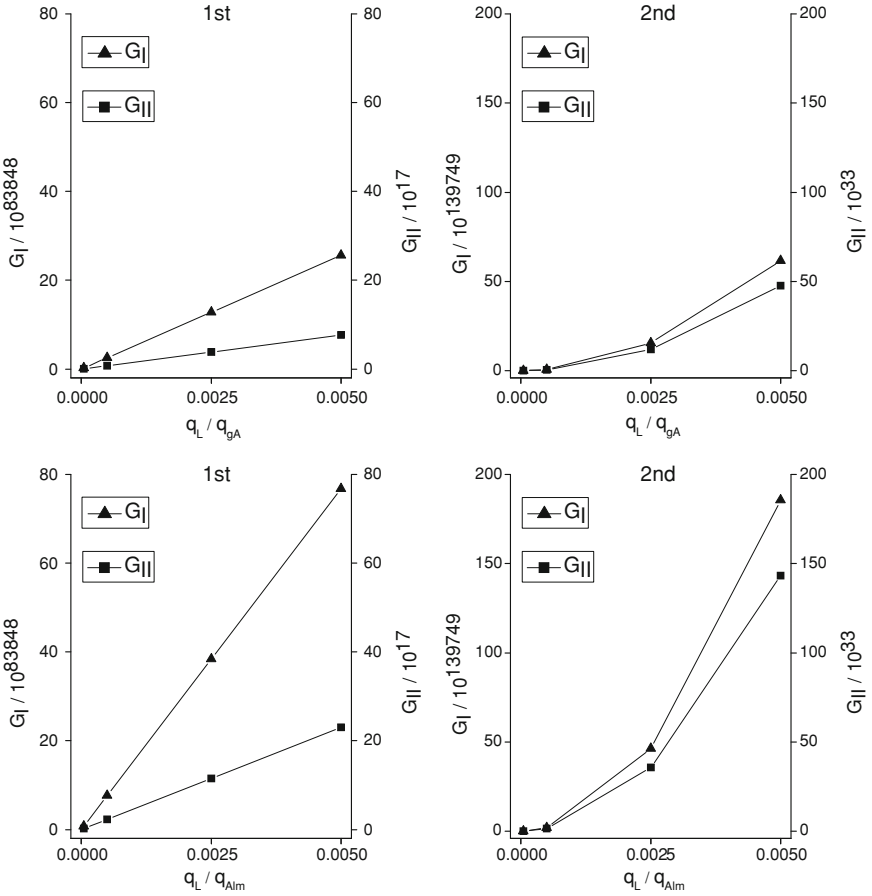

Fig. 5.19 Energy (G_I and G_{II}) as a function of q_L/q_{gA} for the gA channel (*upper panel*) or q_L/q_{Alm} for the Alm channel (*lower panel*) in lipid bilayer energetics in the first- and second-order of lipid screening, respectively. Here, $r_{\mathrm{LL}} = 7.74597\,\text{Å}$

$$F_{\mathrm{dis}} \propto \exp(d_0 - l) \tag{5.32}$$

which is very different from the dissociation force calculated based on the bilayer elastic model [38, 40, 66, 67] where F_{dis} on a gA channel has been reported to change linearly with the change of $d_0 - l$ (see Eq. 5.12 for comparison) [6, 13].

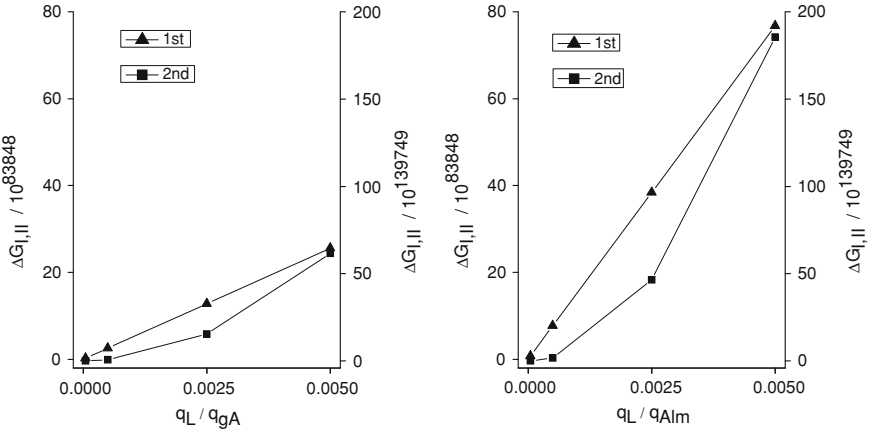

Fig. 5.20 Plot of $\Delta G_{I,II}$ as a function of q_L/q_{gA} (*left panel*) or q_L/q_{Alm} (*right panel*) in lipid bilayer energetic in the first- and second-order of lipid screening. Here, $r_{\mathrm{LL}} = 7.74597\,\text{Å}$

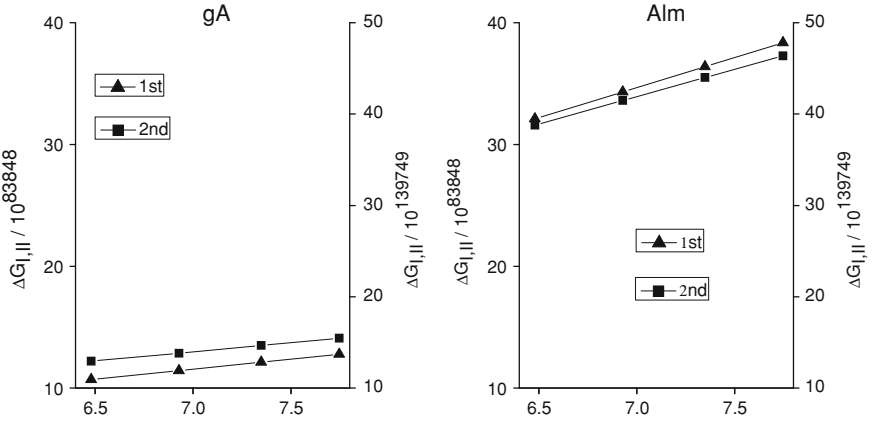

Fig. 5.21 Plot of $\Delta G_{I,II}$ as a function of r_{LL} for the gA channel (*left panel*) and the Alm channel (*right panel*) in lipid bilayer energetics in the first- and second-order of lipid screening, respectively. Here, $q_L/q_M = 0.0025$

5.6 Fitting Theoretical Predictions to Experimental Results

The experimental results presented in Sect. 5.4 show that the gA channel's lifetime τ decreases drastically as the bilayer thickness increases, and at a sufficiently high thickness, the gA channel structure experiences a conformational transition. The trend in the value of τ in a PC bilayer shows that it decreases almost exponentially with the increase of bilayer thickness. A recent study [6] has also supported this conclusion that τ decreases almost exponentially with the increase of the bilayer-channel hydrophobic mismatch. Within a reasonable approximation, since it can

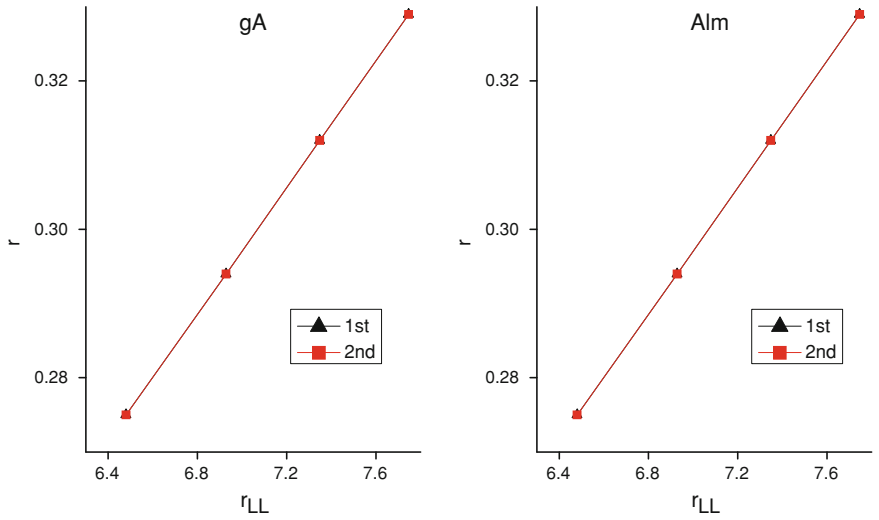

Fig. 5.22 The reaction coordinate which was used in the plot of $\Delta G_{I,II}$ as a function of r_{LL} for the gA channel (*left panel*) and Alm channel (*right panel*) in lipid bilayer energetics in the first- and second-order of lipid screening, respectively. Here, $q_L/q_M = 0.0025$

be assumed that the gA channel stability decreases with the increase of the bilayer induced dissociation force, we conclude that $\tau \propto \exp(-(d_0 - l))$. Considering the theoretical value of F_{dis} in Eq. 5.13, this experimental channel lifetime relation with the mismatch is supported by a previously presented derivation of gA channel lifetime (Eq. 5.27) in a continuum distribution of local energy traps [85] which is also borne out elsewhere [6, 56].

Another possibility is to use the traditional way of deriving lifetime, using the relation presented in Eq. 5.13. Slight differences in the bilayer thickness gA channel length mismatch dependence of the theoretical trend of gA channel lifetime appear to depend on whether we use the expression for F_{dis} from the screened Coulomb model ($\sim \exp(d_0 - l)$), or the elastic bilayer model ($\sim (d_0 - l)$) in the case when c_0 is assumed to be unchanged. In both of these cases the theoretical channel destabilization increases (lifetime τ_{th} decreases) exponentially at small values of $d_0 - l$ but as $d_0 - l$ increases, higher channel destabilization is observed in the former case compared to the latter case (see Fig. 5.24). For any constant thermodynamic condition, the average channel lifetime therefore changes as a negative exponential function (or more strongly) of the hydrophobic mismatch between the bilayer thickness and channel length.

The origin of this difference is readily found if we expand the exponential expression (screened Coulomb model) in a power series as:

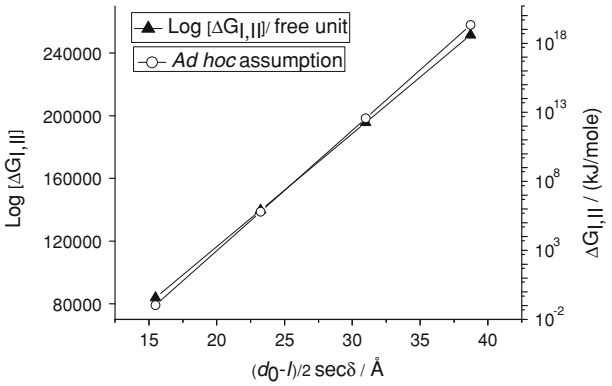

Fig. 5.23 Plot of Log$[\Delta G_{I,II}]$ as a function of $d_0 - l$. Here, $(d_0 - l)$ sec δ is the distance covered by the lipid head groups in the deformed regions of the bilayer at the bilayer gA channel interaction sites. δ(for simplicity, they can be assumed to appear with a constant value within $0-90^\circ$ in a particular lipid bilayer membrane for all participating lipids in all orders of screening at the gA channel bilayer interface), the angle at which lipids in the deformed portion of the bilayer couple with the extension of the gA channel length. $\Delta G_{I,II}$ increases exponentially with $d_0 - l$. $\Delta G_{I,II}$ at lower values of $d_0 - l$ (e.g., $d_0 - l \approx 0$) or at other higher values of $d_0 - l$ can be extrapolated from the plot. For a certain type of lipid with a fixed lipid charge, $\Delta G_{I,II} \propto \exp(d_0 - l)$. Consequently, the dissociation force imposed by the bilayer on the gA channel (F_{dis}) increases exponentially with $d_0 - l$, i.e., $F_{\text{dis}} = -\left(-\frac{\partial \Delta G_{I,II}(d_0-l)}{\partial(d_0-l)}\right) \propto \exp(d_0 - l)$. As a result, the gA channel lifetime decreases exponentially with the increase of $d_0 - l$. *Ad hoc* assumptions ($q_{\text{gA}} \sim$ electron charge and other relevant parameters [1, 16, 17, 35, 41, 71, 75] give an estimate of $\Delta G_{I,II}$ / (kJ/mole) which strongly depends on q_L as d_0 increases. Results in previous figure fall within the second-order screening ($d_0 - l < 40$ Å). Experimentally, this was observed in previously published data [6, 56] and here in the experimental results section

$$\begin{aligned}\Delta G_{I,II} = \mathrm{e}^{(d_0-l)} &= \frac{(d_0-l)^2}{2} + \left(1 + (d_0-1) + \frac{(d_0-1)^3}{6} + \frac{(d_0-1)^4}{24} + \ldots\right) \\ &= \Delta G_{I,II}(\text{Harm}) + \Delta G_{I,II}(\text{A.Harm}). \end{aligned} \tag{5.33}$$

The symbols Harm and A.Harm denote the harmonic and anharmonic contributions in $\Delta G_{I,II}$, respectively. The necessity to include $\Delta G_{I,II}$(A.Harm) is generally expected in the case with higher values of $d_0 - l$ (see Fig. 5.21) whereas the elastic bilayer theory predicts the presence of only a harmonic term $\sim (d_0 - l)^2$ in the bilayer deformation energy, which is adequate for sufficiently small deformation values. This is also readily found in the screened Coulomb energy. Consequently, $F_{\text{dis}} = \frac{\partial}{\partial(d_0-l)} \Delta G_{I,II}$ in the screened Coulomb model also contains additional terms (different orders) besides the term $(d_0 - l)$, which is the only geometric mismatch term found in the elastic bilayer theory to regulate the change of the gA channel lifetime (in the case of non-changing lipid curvature profiles). Although both the screened Coulomb model and the elastic bilayer model calculations generally suggest an exponential damping in gA channel lifetime with increasing $d_0 - l$ which is consistent with the experimental data presented in Sect. 5.4 (and in [6, 56]), the

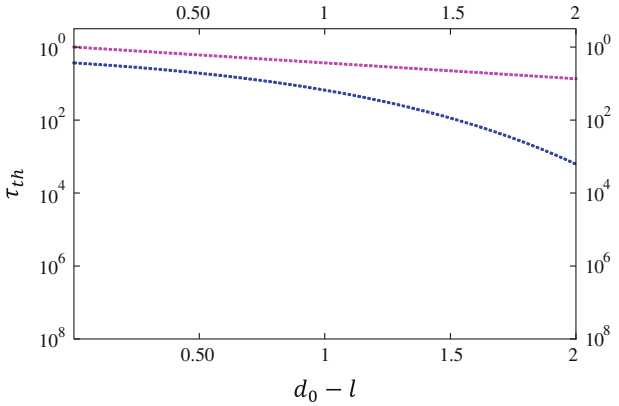

Fig. 5.24 Plot of theoretical values of gA channel lifetime τ_{th} (arbitrary units, using $\tau_{\text{th}} \sim e^{-\frac{(\lambda^+ - \lambda)F_{\text{dis}}}{k_B T}}$, Eq. 5.13) as a function of the bilayer thickness gA channel length mismatch $d_0 - l$ (arbitrary units). The *lower curve* represents τ_{th} using the screened Coulomb theory while the upper curve represents τ_{th} derived from the elastic bilayer theory, both explained earlier. In both plots $\lambda^+ - \lambda$ is considered constant. Both curves are straight lines (in log-lin plot) meaning τ_{th} drops exponentially with increasing $d_0 - l$ at the low mismatch level but τ_{th} (from the screened Coulomb formula) drops even faster (lower curve) as $d_0 - l$ increases due to the inclusion of anharmonic terms (explained earlier and in Fig. 5.25) in the energy at high values of mismatch

screened Coulomb model calculation hints at the presence of extra damping, due to higher order anharmonic terms in the energy expression. This better explains why at high mismatch values, the channel experiences not just destabilization but also structural transitions (see Sect. 5.4) due to the energetic cost of the super-heavy bilayer deformation energy (see Fig. 5.23). We therefore conclude that although the elastic bilayer model [38, 40] which yields the deformation energy dependence according to $\sim(d_0 - l)^2$ [6, 13] may be applicable in the small deformation limit, it requires a modification for values outside this limit. For the same reason, the theory based on a linear spring approximation for the coupling between the bilayer and gA channels [57], which explicitly shows an exponential damping of gA channel lifetime with an increasing $d_0 - l$, can be a very good approximation when $d_0 - l$ is relatively small. However, when $d_0 - l$ is large enough and the interaction between a gA channel and the bilayer extends to other next-neighbor lipids in the deformed regions of the bilayer near the channel, an extension of the elastic model is warranted.

Theoretical and experimental results also show identical trends in the regulation of the gA channel stability induced by the lipid curvature properties. The energy barriers modestly change due to the change of the lipid-lipid separation r_{LL} (determined from the square root of the average lipid cross-sectional area in a bilayer) which changes as the lipid curvature changes. For simplicity, in the theoretical analysis we have assumed the same value of r_{LL} for both the lipid-lipid separation and the lipid-peptide separation at the channel bilayer interface. The energy barrier also shows a modest change due to the change of lipid charge. To some extent, lipid charge also

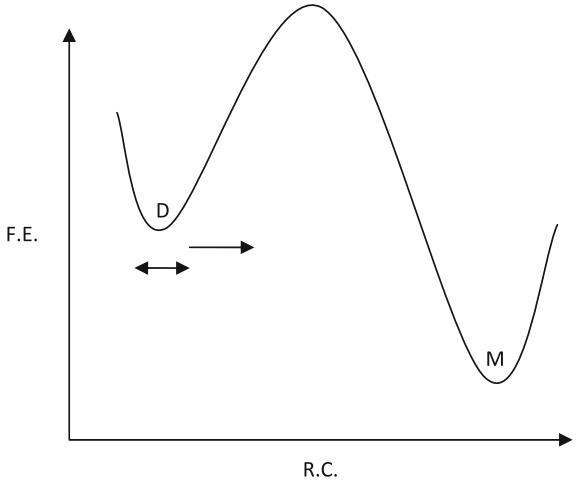

Fig. 5.25 Schematic illustration showing the free energy (F.E.) dependence on the reaction coordinate (R.C.) when protein conformational transitions between different energy states occur. The back-and-forth transitions between gA dimer (D) and monomers (M) have been demonstrated here. These states have different energy values and are separated by a potential barrier. $\Delta G_{I,II}$(Harm) and $\Delta G_{I,II}$(A.Harm) energy terms are effective in the small deformation (bi-directional arrow in the figure, within a very short range from the point of the energy minimum, thanks to harmonic behavior) and beyond the small deformation region (*right arrow*), respectively, to ensure transitions from D to M states and vice versa of gA. Only in the limit of extremely small bilayer deformation ($d_0 - l \sim 0$) the inclusion of only the harmonic term $\Delta G_{I,II}$(Harm) $\sim (d_0 - l)^2$ may be sufficient. When $d_0 - l$ increases beyond the immediate vicinity of the free energy minima, higher order anharmonic energy terms dominate in the transition between D and M states. All such energy states appear together in the screened Coulomb interaction model calculation but are missing in the elastic bilayer model calculation of the bilayer deformation energy as explained in the text

determines the lipid curvature properties. Hence, the change in the lipid charge also regulates the gA channel functions in lipid bilayers. The model calculation hints for a stronger lipid charge effect on gA channel stability in the case of higher values of $d_0 - l$ (see Eq. 5.29).

The experimental data for the Alm channel in a lipid bilayer also show considerable agreement with the results of the theoretical model (see Figs. 5.17 and 5.18). To initiate the formation of an Alm channel under the experimental conditions mentioned in Sect. 5.4, a minimum peptide concentration of $\sim 10^{-8}$ M is required [12]. However, once the Alm channel starts forming, we observe that the Alm channel activity increases considerably with the increase of $[M_{\text{Alm}}]$. These data are in good agreement with the theoretical prediction of channel activity depending mainly on $\Delta G_{I,II}$ in the initiation phase. Once the channels start forming, the bilayer's physical parameters which determine $\Delta G_{I,II}$ appear to be very critical in the regulation of the channel formation mechanism and the channel formation rate sharply increases with peptide concentration. We have also experimentally observed that the detailed Alm channel activity shows considerable dependence on bilayer thickness and on lipid

curvature. Higher lipid charges strongly destabilize the probability of observing any Alm channel current level, especially higher order current levels [18]. The higher concentration $[M_{\mathrm{Alm}}]$ required in thicker bilayers or bilayers containing lipids with negative curvature or charges are likely to change the free energy profile in bilayers [92] which compensates for the changed values of the theoretically calculated $\Delta G_{I,II}$. The experimentally observed changes in free energies $\Delta G^{1\to 2}$ and $\Delta G^{1\to 3}$ of any Alm channel within a lipid bilayer system are not drastically different, which is consistent with the calculated values of $\Delta G_{I,II}$ for any specific order of lipid screening where the values of $\Delta G_{I,II}$ do not considerably change due to the change of the number of monomers in Alm channels. In particular, $\Delta G_{I,II}$ values stay within the same order of magnitude but slightly increase with the increase of the number of Alm monomers participating in Alm channel formation mainly due to the increased channel-bilayer interaction sites. However, $\Delta G_{I,II}$ changes exponentially between different lipid orders which can be compared with the compensation of free energy changes [92] due to the requirement of higher geometric orders of $[M_{\mathrm{Alm}}]$ (or $[M_{\mathrm{gA}}]$ in the case of gA channels) when the bilayer thickness increases or neutral lipids are replaced by more negative curvature bearing lipids in the bilayers.

5.7 Evidence of Physical Interactions Between Lipids and Channel-Forming Peptides or Other Drugs: A Case Study Using Molecular Dynamics Simulations

We designed an *in silico* molecular dynamics (MD) simulation [15] in order to model the drug-lipid interactions and to gain deeper insights into the problem. This simulation illustrates how an empirical calculation of the force field finds partial charges on each atom in the drugs or peptides interacting with lipids on lipid membranes, irrespective of their net molecular charges [24, 43, 44, 53].

In charge-bearing peptide-induced ion channels, e.g., gA and Alm, or charge-neutral chemotherapy drug-induced ion pores [14], both ion channel/pore forming agents and lipids approach each other through hydrophobic coupling (e.g., see Figs. 5.2, 5.6, 5.7, 5.8, 4.5, etc.). So naturally, charges on charge-bearing lipids e.g., phophatidylserine (PS), phosphatidylglycerol (PG), etc. and charge-bearing peptides, e.g., gA, Alm, etc. experience electrical fields created by each other. But what happens if both lipids and channel-forming drugs have no net molecular charges? This question naturally appears as most of the lipids in cell membranes are zwitterionic phosphatidylcholines (PCs) with no net electric charges. Also, the finding of channel formation by charge neutral chemotherapy drugs [14] raises the question if there is any possibility to observe interactions between the channel-forming drugs and bilayer constituents, especially lipids, due to the electrical properties of drugs and lipids in a manner equivalent to the claimed peptide lipid screened Coulomb interactions in gA channels lipid bilayer binding ([11] in Chap. 4). To clearly understand this general issue we have performed MD simulations.

5.7.1 MD Techniques

We considered five different relative locations and orientations randomly generated in each drug-lipid complex as initial structures for MD simulations. For each location- and orientation-specific complex, a 6 ns (chemotherapy drugs) or 10 ns (gA or Alm) explicit water MD simulation at 300 K in a solution at pH 7 was performed. We applied the software package Amber 11 [84], specifically the Amber force field ff03 was used. The explicit water TIP3P model was used to simulate solvent effects. The force field parameters for drugs and lipids (PC and PS) were generated using an Amber module antechamber [28, 77]. Twenty complexes were energy-minimized using the steepest descent method for the first ten cycles, and then followed by a conjugate gradient for another one thousand cycles. We then applied Langevin dynamics during the process of heating up the system for 200 ps with the energy-minimized complex, in which drug and lipid molecules were being restrained using a harmonic potential with a force constant $k = 100$ N/m. Afterward, we introduced pressure regulation to equilibrate water molecules around the complex, and to reach an equilibrium density for another 200 ps in addition to temperature regulation. The MD production run then was continued for 6 ns. Note that the phospholipid was gently restrained with a harmonic potential with a force constant $k = 10$ N/m, applied only to the phosphate during the production runs.

5.7.2 MD Results and Discussion

The Drug/Peptide Lipid Physical Interactions as a Possible Cause of Their Induced Pore Formation

MD results presented in Figs. 5.26 and 5.27 suggest that the drug/ peptide lipid complex fluctuates within a separation over a period of time. These results suggest that both drugs and peptides likely bind with PC and PS given appropriate initial conditions [15]. In the in-depth analysis, we found evidence suggesting that the hydrophobic effect is unlikely to contribute into the distance dependent drug/peptide lipid binding. The analysis of energy contributions from two non-bonded interactions, E_{vdW} and E_{ES} versus $d_{\mathrm{drug-lipid}}$ revealed crucial insights into the cause of the observed stability of the drug/peptide lipid complexes. Both E_{vdW} and E_{ES} appear to be the main contributors to the energetic drug/peptide lipid binding and vdW interactions contribute slightly more than ES interactions as the drug and lipid approach closer. Binding stability generally is found to decrease quickly with increasing $d_{\mathrm{drug-lipid}}$. Both vdW and ES interactions contribute comparably with both energies decreasing with increasing $d_{\mathrm{drug-lipid}}$. Large standard deviations (Figs. 5.26 and 5.27) are suggestive of the conformational space of the drug/peptide lipid complexes not being completely explored in MD simulations. Nonetheless, this incompleteness does not preclude the proposed interpretation. Importantly, the drug/peptide

lipid interactions resemble the protein lipid vdW and ES interactions found in MD simulations of a gA channel in phospholipid membranes [91].

These results suggest that the observed vdW and ES binding energies, which presumably arise from the electrical properties of both of the participating agents, do not depend on the molecular net charges. We observe the presence of both vdW and ES, even in cases where either or both of the participating agents (e.g. PC, chemotherapy drugs, etc.) have no net molecular charges. Therefore, it is clear that the interactions appear due to the partial charges on each atom in the drugs or peptides interacting with lipids on lipid membranes, irrespective of their net molecular charges [24, 43, 44, 53]. This hypothesis has appeared in the screened Coulomb interaction model through the consideration of the localized charges on the participating agents, irrespective of the consideration of their net molecular charges.

5.8 Discussion and Conclusions

In this chapter, we have investigated the issue of how the hydrophobic coupling between a lipid bilayer and integral channels regulates the channel stability, using two structurally different gramicidin A and alamethicin channels as primary examples. Conformational changes of both trans-bilayer dimerized linear gramicidin A channels and 'barrel-stave' pore type alamethicin channels are regulated mainly by the bilayer channel coupling energetics. Experimental results show that an increased hydrophobic mismatch between bilayer thickness and channel length ($d_0 - l$) appears as a major channel destabilizing factor. Increased negative lipid curvature and lipid charge also induce considerable destabilization into channel formation. To theoretically address the observed lipid bilayer-induced regulation of channel stability, we have developed a simple physical model of the 'screened Coulomb interaction', which has been used to calculate the binding energy of a gramicidin A dimer with a lipid bilayer required for the stability of the channel structure. The model calculates the binding energy, considering mainly the electrical properties of both the lipids on the bilayer and the channel-forming agents. The same model can be extended to also calculate the binding energy of an alamethicin channel with a lipid bilayer. In this screened Coulomb interaction model, the calculation of the binding energy of a channel with a lipid bilayer considers most of the relevant properties such as the localized charges of both peptides and lipids, geometry of the environment (bilayer thickness, channel length, channel cross-sectional area, lipid head group cross-sectional area, lipid intrinsic curvature), the change in the dielectric constant (relative to the aqueous phase) of the hydrophobic region near the channel interface, and a specific mechanical property such as bilayer elasticity. Changes in any of these properties modulate the binding energy between the bilayer and the channel, which alters the channel's stability. We have compared the model results directly with the experimental results on stability and energetics of the gramicidin A and alamethicin channels in lipid bilayers, and have found them to be in very good agreement.

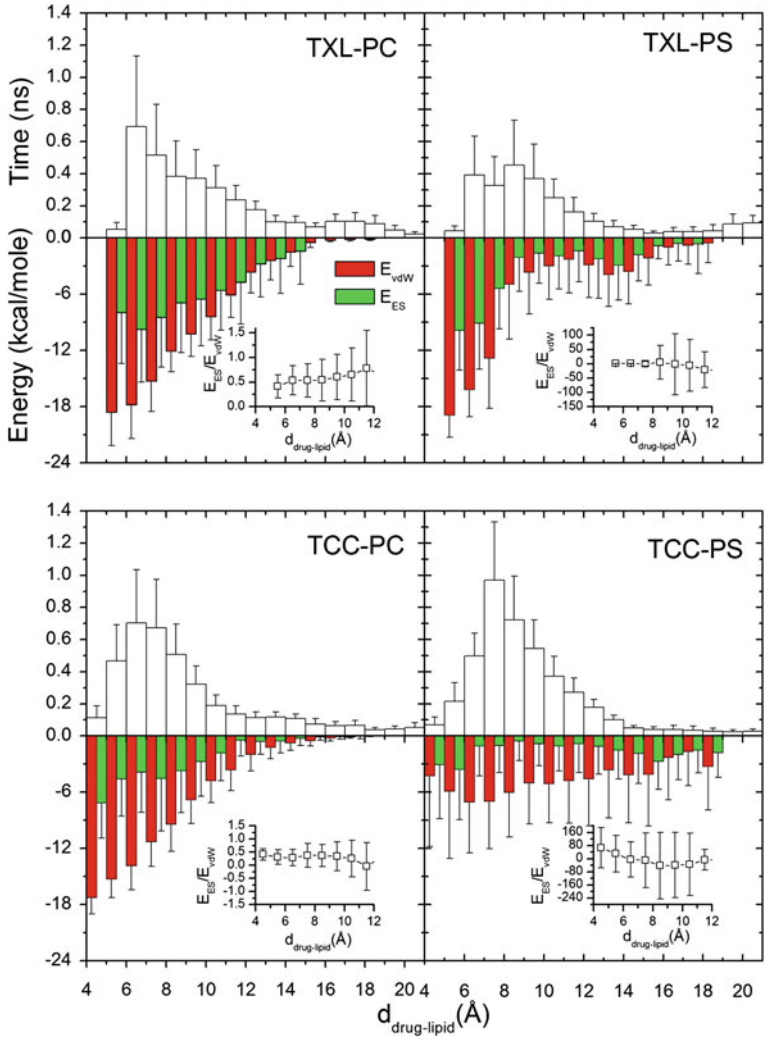

Fig. 5.26 In all the histograms (*upper panel*) of time versus $d_{\text{drug}-\text{lipid}}$, the duration of the drug/lipid complex staying together (height) within a distance (width) in 6 ns MD simulations is presented. *Lower panels* show the histograms of non-bonded van der Waals (vdW) energy (E_{vdW}) and electrostatic (ES) interaction energy (E_{ES}). To avoid color conflict, E_{vdW} and E_{ES} are shown to occupy half–half widths although each half represents the whole width of the corresponding histogram

The calculations using screened Coulomb interactions demonstrate that the bilayer deformation energy ($\Delta G_{I,II} \approx \Delta G^0_{\text{def}}$) increases by orders of magnitude with the increase of the order of the lipid screening. The increasing lipid screening order is a measure of the hydrophobic bilayer thickness channel length mismatch, due to either an increase in bilayer thickness or decrease in channel length, or both.

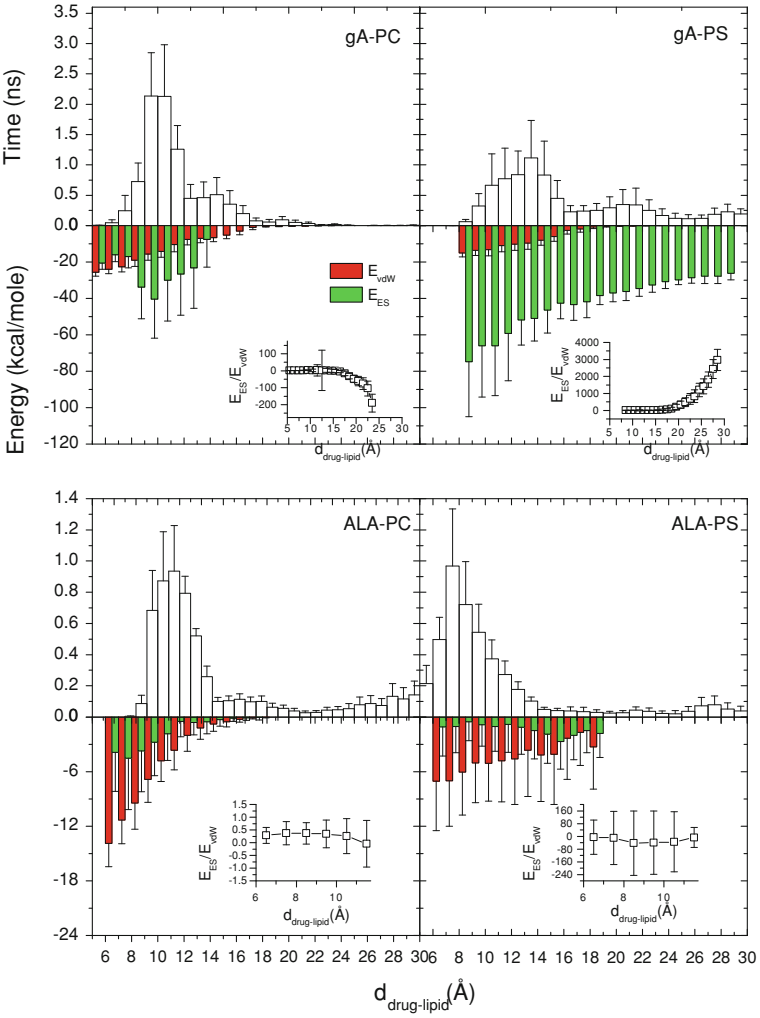

Fig. 5.27 In all the histograms (*upper panel*) of time versus $d_{\text{drug}-\text{lipid}}$, the duration of the drug/lipid complex staying together (height) within a distance (width) in 6 ns MD simulations is presented. *Lower panels* show the histograms of non-bonded van der Waals (vdW) energy (E_{vdW}) and electrostatic (ES) interaction energy (E_{ES}). To avoid color conflict, E_{vdW} and E_{ES} are shown to occupy half–half widths though each half represents the whole width of the corresponding histogram

Other studies using β-helical gramicidin A channels [7] and α-helical peptides like acetyl-GWW(LA)$_n$LWWA-amide (WALP) [47, 48], incorporated in lipid bilayers with different thicknesses, provide experimental evidence for the response between bilayer and protein structural alterations and the hydrophobic mismatch. An increase in the values of $\Delta G_{I,II}$ causes destabilization of the corresponding channels. Therefore, the stability or the average lifetime of a channel can decrease by decreasing

the channel length or increasing the bilayer thickness. The experimental results fit perfectly with the trends found in the theoretical model. A shorter gramicidin A channel (gA-(13)) is experimentally observed to be less stable than a longer gramicidin A channel (AgA(15)), or both of these channels are exponentially less stable in a thicker ($DC_{20:1}PC$) bilayer than in a thinner ($DC_{18:1}PC$) one. Other important parameters in the theoretical model are the intrinsic lipid curvature and the lipid charge. An increased effective lipid cross-sectional area is a result of either a higher negative curvature, e.g. PE's over PC's, or the lipid head group charges causing Coulomb repulsion between lipids. The model calculation shows that increased lipid cross-sectional areas ($\sim r_{\mathrm{LL}}^2$) result in a modest increase in $\Delta G_{I,II}$, which makes the channel formation harder so the lifetime of a channel decreases. The experimental results show that gramicidin A channel lifetimes in a negative curvature-bearing DOPE bilayer are shorter than those in a neutral $DC_{18:1}PC$ bilayer: the effect of negative curvature induces linear destabilization in gramicidin A channels. As the value of r_{LL}^2 increases with the increase in lipid intrinsic curvature, we conclude that a very good agreement exists between the theoretical predictions and experimental observations. Using the theoretical expression for the channel-bilayer binding energy, one can also derive the elastic force constants and consider higher order effects on elastic force constants with an increased value of s (representing a higher mismatch) exactly illustrating the effects of lipid charges, as shown in Eq. 5.29. Thus, an increased bilayer elasticity helps the bilayer to deform near the channels. Despite elasticity effects being secondary relative to the charge effects, the increased bilayer elasticity reduces the bilayer deformation energy which favors the stability of a channel in a bilayer membrane. Higher values of s, corresponding to a higher mismatch $d_0 - l$, also indirectly confirm that an equal increase in bilayer elasticity reduces $\Delta G_{I,II}$ for shorter gramicidin A channels (accounting for a larger mismatch) more than that for longer gramicidin A channels (accounting for a smaller mismatch). As a result, stability of shorter gramicidin A channels increases relatively more strongly than that of longer gramicidin A channels. The experimental studies [10, 11, 13] claimed to induce increased elasticity into bilayers by bilayer-active amphipathic molecules, such as several anti-fusion peptides, amphiphiles like triton X-100 and capsaicin, and even an antimicrobial peptide gramicidin S. They also demonstrated that channels generally show higher stability with an increase of the elasticity of the lipid bilayers. Furthermore, in [13] it was shown that by increasing bilayer elasticity, the bilayer deformation energy is reduced which in the model calculation appears as a decrease in $\Delta G_{I,II}$. Requirements of higher gramicidin A and alamethicin concentrations in both thicker bilayers and more negative-curvature bearing PE bilayers over PC bilayers also confirm that a higher mismatch between the bilayer's hydrophobic thickness and channel length and negative lipid curvature are two very important regulators of channel functions, which the theoretical model predicts and experimental results confirm.

In this chapter, we have developed a theoretical model for bilayer channel energetics based on experimentally measurable values of general physical properties, such as charge and size of the channel-forming peptides and the bilayer constituents e.g. mainly lipids. By considering a simple model of screened Coulomb

interactions, we have formulated a relatively simple and tractable method, and avoided the previously encountered complications in a method of calculating the elastic bilayer deformation energy [21, 38, 40, 66, 67, 74] based on the assumption of complicated individual contributions from the intrinsic monolayer curvature, local compression and bending moduli of two bilayer leaflets, and the associated energy densities [34, 63]. The molecular dynamics simulations of gramicidin A in lipid bilayers utilizing an all-atom force field [2] and computation of the potential of mean force in a lipid mediated protein-lipid hydrophobic coupling [23] helped us confirm that the lipid head group region effectively regulates the lipid bilayer gramicidin A channel hydrophobic coupling. The acyl chains may also produce some direct partial pressure profile on the gramicidin A channels at the channel bilayer interaction sites, but that should be averaged out by their contributions from all sides of a gramicidin A channel. One very important insight gained through the model is that the bilayer imposed dissociation force on gramicidin A channel increases (and as a result, the gramicidin A channel lifetime decreases) at least exponentially, which matches with the experimental observations (see Fig. 5.3 and [6, 56]). The experimental observation of increasing the negative lipid curvature-induced linear decrease in gramicidin A channel stability verified by the theoretical results also provides evidence in favor of the approach of regulating membrane protein functions due to the hydrophobic energetic membrane–membrane protein coupling. In the alamethicin channel, the requirement of higher orders of concentration $[M_{\mathrm{Alm}}]$ in thicker lipid bilayers may compensate for the huge variation in $\Delta G_{I,II}$, but the experimentally observed small changes in the free energies $\Delta G^{1\to 2}$ and $\Delta G^{1\to 3}$ of any alamethicin channel within a lipid bilayer system correspond to a little variation in the theoretical values of $\Delta G_{I,II}$ for alamethicin channels consisting of different numbers of monomers. It should also be stressed that the model calculation is valid for an arbitrary hydrophobic mismatch between bilayer thickness and channel length and is equally applicable to at least two types of protein-lined channels, i.e. linear β-helical gramicidin A type and 'barrel-stave' pore alamethicin type. We have found very good agreements between the results on channel stability/lifetime emerging from the binding energy calculation using screened Coulomb interactions and the experimental observations on gramicidin A and alamethicin channels. The molecular dynamics simulations also suggest the presence of distance-dependent electrostatic and van der Waal's interactions between lipids and membrane active agents (peptides or other biomolecules like chemotherapy drugs, nucleic acid oligomers, or aptamers, etc.). These simulation results also support the existence of interactions between the membrane and active agents, due primarily to their electrical properties. The use of the screened Coulomb interaction model in the membrane–membrane protein energetics is also supported by molecular dynamics simulations. This theoretical screened Coulomb interaction model calculation can therefore be generally applied to the energetics and dynamics of several kinds of membrane proteins with a variety of membrane effects, as long as they are hydrophobically coupled with lipid bilayers.

Finally, we conclude that the physical lipid-membrane protein interactions, due mainly to their electrical properties and the related energetics, appear as primary regulators of membrane protein functions. A membrane's elasticity helps it to bend, due

to the pull originating primarily from the electrostatic and van der Waal's interactions between localized charges on lipids and membrane proteins or any other membrane-active drug molecules. Both electrical energetic coupling (primary regulator) and mechanical energetic coupling (secondary regulator) between a lipid bilayer and integral membrane proteins regulate the membrane protein functions.

References

1. Aguilella, V. M. and Bezrukov, S. M.: Alamethicin channel conductance modified by lipid charge. Eur. Biophys. J. **30**, 233–241 (2001).
2. Allen, T. W., Andersen, O.S. and Roux, B.: Energetics of ion conduction through the gramicidin channel. Proc. Natl. Acad. Sci. **101**, 117–122 (2004).
3. Andersen, O.S., D. B. Sawyer and Koeppe, R.E. II. In: Biomembrane structure and Function, K. R. K. Easwaran and B. Gaber (eds.) p227. Schenectady, New York: Adenine (1992).
4. Andersen, O.S.: Ion movement through Gramicidin A Channels - Studies on the Diffusion-controlled Association Step. Biophys. J. **41**, 147–165 (1983).
5. Andersen, O.S., Nielsen, C., Maer, A. M., Lundbæk, J. A., Goulian, M. and Koeppe, R.E. II: Gramicidin channels: molecular force transducers in lipid bilayers. Biol. Skr. Dan. Vid. Selsk. **49**, 75–82 (1998).
6. Andersen, O.S. and Koeppe, R.E. II: Bilayer thickness and membrane protein function: an energetic perspective. Annu. Rev. Biophys. Biomol. Struct. **36**, 107–130 (2007).
7. Andersen, O.S., Koeppe, R.E. II and Roux, B.: Gramicidin Channels. IEEE Trans. Nanobiosci. **4**, 10–20 (2005).
8. Arseniev, A. S., Barsukov, I. L., Bystrov, V.F. and Ovchinnikov, Yu. A.: Biol. Membr. **3**, 437 (1986).
9. Ashrafuzzaman, M. and Beck, H.: In Vortex dynamics in two-dimensional Josephson junction arrays, University of Neuchatel, ch 5 p 85, (2004) http://doc.rero.ch/record/2894ln=fr
10. Ashrafuzzaman, M. and Andersen, O.S.: Lipid bilayer elasticity and intrinsic curvature as regulators of channel function: a single molecule study. Biophys. J. **421A** (2007).
11. Ashrafuzzaman, M., McElhaney, R. N. and Andersen, O.S.: One antimicrobial peptide (gramicidin S) can affect the function of another (gramicidin A or alamethicin) via effects on the phospholipid bilayer. Biophys. J. **94** 6–7, (2008).
12. Ashrafuzzaman, M., Andersen, O.S. and McElhaney, R. N.: The antimicrobial peptide gramicidin S permeabilizes phospholipid bilayer membranes without forming discrete ion channels. Biochim. Biophys. Acta **1778**, 2814–2822 (2008).
13. Ashrafuzzaman, Md., Lampson. M.A., Greathouse, D.V., Koeppe II, R.E., Andersen, O.S.: Manipulating lipid bilayer material properties by biologically active amphipathic molecules. J. Phys.: Condens. Mat. **18**, S1235–1255 (2006).
14. Ashrafuzzaman, Md., Duszyk, M. and Tuszynski, J. A.: Chemotherapy drugs Thiocolchicoside and Taxol Permeabilize Lipid Bilayer Membranes by Forming Ion Pores. J. of Physics: Conf. Series **329**(012029), 1–16 (2011).
15. Ashrafuzzaman, Md., Tseng, C.-Y., Duszyk, M. and Tuszynski, J. A.: Chemotherapy drugs form ion pores in membranes due to physical interactions with lipids. submitted (2011).
16. Benz, R., Fröhlich, O., Läuger, P., and Montal, M.: Electrical capacity of black lipid films and of lipid bilayers made from monolayers. Biochim. Biophys. Acta **394**, 323–334, (1975).
17. Berneche, S. and Roux, B.: Molecular Dynamics of the KcsA K^+ Channel in a Bilayer Membrane. Biophys. J. **78**, 2900–2917 (2000).
18. Bezrukov, S.M., Rand, R.P., Vodyanoy, I. and Parsegian, V. A.: Lipid packing stress and polypeptide aggregation : alamethicin channel probed by proton titration of lipid charge. Faraday Discuss. **111**, 173–183 (1998).

19. Boheim, G.: Statistical analysis of alamethicin channels in black lipid membranes. J. Mem. Biol. **19**, 277–303 (1974).
20. Brown, M.F.: Modulation of rhodopsin function by properties of the membrane bilayer. Chem. Phys. Lipids **73**, 159–180 (1994).
21. Dan, N. and Safran, S.A.: Effect of Lipid Characteristics on the structure of Trans-membrane proteins. Biophys. J. **75**, 1410–1414 (1998).
22. Daune, M.: Molecular Biophysics: structures in Motion, Oxford University Press, Oxford (1999).
23. de Meyer, F. and Smit, B. Comment on "cluster formation of trans-membrane proteins due to hydrophobic mismatching". Phys. Rev. Lett. **102**, 219801 (2009).
24. Duan, Y., Wu, C., Chowdhury, S., Lee, M.C., Xiong, G., Zhang, W., Yang, R., Cieplak, P., Luo, R., Lee, T.: A point-charge force field for molecular mechanics simulations of proteins based on condensed-phase quantum mechanical calculations. J. Comput. Chem. **24**, 1999–2012 (2003).
25. Durkin, J. T., Koeppe, R.E. II and Andersen, O.S.: Energetics of gramicidin hybrid channel formation as a test for structural equivalence *1: Side-chain substitutions in the native sequence. J. Mol. Biol. **211**, 221–234 (1990).
26. Durkin, J. T., Providence, L. L., Koeppe, R.E. II and Andersen, O.S.: Energetics of heterodimer formation among gramicidin Analogues with an NH_2-terminal addition or deletion consequences of missing a residue at the join in the channel. J. Mol. Biol. **231**, 1102–1121 (1993).
27. Evans, E. A. and Hochmuth, R.M.: Curr. Top. Membr. Transp. **10**, 1 (1978).
28. Evans, E., Rawicz, W. and Hofmann, A.F.: In Bile Acids in Gastroenterology Basic and Clinical Advances, edited by A.F. Hofmann, G. Paumgartner and A. Stiehl (Dordrecht: Kluwer-Academic), p 59 (1995).
29. Finkelstein, A.: Water and nonelectrolyte permeability of lipid bilayer membranes. J. Gen. Physiol. **68**, 127–135 (1976).
30. Goulian, M., Mesquita, O.N., Fygenson, D.K., Nielsen, C., and Andersen., O.S.: Gramicidin channel kinetics under tension. Biophys. J. **74**, 328–337 (1998).
31. Greathouse, D. V., Koeppe, R.E. II, Providence, L. L., Shobana, S. and Andersen, O.S.: Design and characterization of gramicidin channels. Meth. Enzymol. **294**, 525–550 (1999).
32. Grønbech-Jensen, N., Mashl, R. J., Bruinsma, R. F., and Gelbart, W. M.: Counterion-induced attraction between rigid polyelectrolytes. Phys. Rev. Lett. **78**, 2477–2480 (1997).
33. Gruner, S. M.: In Biologically Inspired Physics, edited by L. Peliti (New York: Plenum), p 127 (1991).
34. Gruner, S. M.: Intrinsic curvature hypothesis for biomembrane lipid composition: a role for nonbilayer lipids. Proc. Natl. Acad. Sci. **82**, 3665–69 (1985).
35. Harper, P.E., Mannock, D.A., Lewis, R.N.A.H., McElhaney, R.N. and Gruner, S.M.: X-Ray diffraction structures of some phosphatidylethanolamine lamellar and inverted hexagonal phases. Biophys. J. **81**, 2693–2706 (2001).
36. He, K., Ludtke, S. J., Huang, H. W. and Worcester, D. L.: Antimicrobial peptide pores in membranes detected by neutron in-plane scattering. Biochemistry **34**, 15614–15618 (1995).
37. Helfrich, W.: Elastic properties of lipid bilayers: theory and possible experiments. Z. Naturforsch. **28C**, 693–703 (1973).
38. Helfrich, P. and Jakobsson, E.: Calculation of deformation energies and conformations in lipid membranes containing gramicidin channels. Biophys. J. **57**, 1075–1084 (1990).
39. Heyer, R. J., Muller, R. U. and Finkelstein, A.: Inactivation of monazomycin-induced voltage-dependent conductance in thin lipid membranes. I. Inactivation produced by long chain quaternary ammonium ions. J. Gen. Physiol. **67**, 703–729 (1976).
40. Huang, H. W.: Deformation free energy of bilayer membrane and its effect on gramicidin channel lifetime. Biophys. J. **50**, 1061–1071 (1986).
41. Hwang, T. C., Koeppe, R.E. II and Andersen, O.S.: Genistein can modulate channel function by a phosphorylation-independent mechanism: importance of hydrophobic mismatch and bilayer mechanics. Biochemistry **42**, 13646–58 (2003).
42. Israelachvili, J.N.: Refinement of the fluid-mosaic model of membrane structure. Biochim. Biophys. Acta **469**, 221–225 (1977).

43. Jakalian, A., Bush, B.L., Jack, D.B., Bayly, C.I.: Fast, efficient generation of high-quality atomic charges. AM1-BCC model: I. Method. J. Comput. Chem. **21**, 132–146 (2000).
44. Jakalian, A., Jack, D.B., Bayly, C.I.: Fast, efficient generation of high-quality atomic charges. AM1-BCC model: II. Parameterization and Validation. J. Comput. Chem. **23**, 1623–1641 (2002).
45. Katsaras, J., Prosser, R. S., Stinson, R. H. and Davis, J. H.: Constant helical pitch of the gramicidin channel in phospholipid bilayers. Biophys. J. **61**, 827–830 (1992).
46. Ketchem, R. R., Roux, B. and Cross, T. A.: High-resolution polypeptide structure in a lamellar phase lipid environment from solid state NMR derived orientational constraints. Structure **5**, 1655–1669 (1997).
47. Killian, J. A. and Nyholm, T. K.: Peptides in lipid bilayers: the power of simple models. Curr. Opin. Struct. Biol. **16**, 473–479 (2006).
48. Killian, J. A., Salemink, I., de Planque, M. R., Lindblom, G., Koeppe, R.E. II, Greathouse, D. V.: Induction of nonbilayer structures in diacylphosphatidylcholine model membranes by trans-membrane alpha-helical peptides: importance of hydrophobic mismatch and proposed role of tryptophans. Biochemistry **35**, 1037–1045 (1996).
49. Kirk, G. L. and Gruner, S. M.: Lyotropic effects of alkanes and headgroup composition on the l_α -H_{II} lipid liquid crystal phase transition : hydrocarbon packing versus intrinsic curvature. J. Phys. **46**, 761–769 (1985).
50. Koeppe, R.E. II, Providence, L. L., Greathouse, D. V., Heitz, F., Trudelle, Y., Purdie, N. and Andersen, O.S.: On the helix sense of gramicidin A single channel. Proteins Struct., Funct., Genet. **12**, 49–62 (1992).
51. Latorre, M. and Alvarez, O.: Voltage-dependent channels in planar lipid bilayer membranes. Physiol. Rev. **61**, 77–150 (1981).
52. Lee, M. T., Hung, W. C., Chen, F. Y. and Huang, H. W.: Many-Body Effect of Antimicrobial Peptides: On the Correlation Between Lipid's Spontaneous Curvature and Pore Formation. Biophys. J. **89**, 4006–4016 (2005).
53. Lee, M.C., Duan, Y.: Distinguish protein decoys by using a scoring function based on a new Amber force field, short molecular dynamics simulations, and the generalized Born solvent model. Proteins **55**, 620–634 (2004).
54. Lewis, B.A. and Engelman, D.M.: Lipid bilayer thickness varies linearly with acyl chain length in fluid phosphatidylcholine vesicles. J. Mol. Biol. **166**, 211–217 (1983).
55. Lundbæk, J. A., Birn, P. H. A. J., Søgaard, R., Nielsen, C., Girshman, J., Bruno, M. J., Tape, S. E., Egebjerg, J., Greathouse, D. V., Mattice, G. L., Koeppe, R.E. II and Andersen, O.S.: Regulation of sodium channel function by bilayer elasticity. The importance of hydrophobic coupling. Effects of micelle-forming amphiphiles and cholesterol. J. Gen. Physiol. **123**, 599–621 (2004).
56. Lundbæk, J. A.: Lipid Bilayer - mediated Regulation of Ion Channel Function by Amphiphilic drugs. J. of Gen. Physiol. **131**, 421–429 (2008).
57. Lundbæk, J.A. and Andersen, O.S.: Spring constants for channel-induced lipid bilayer deformations. Estimates using gramicidin channels. Biophys. J. **76**, 889–895 (1999).
58. Ly, H. V. and Longo, M. L.: The Influence of Short-Chain Alcohols on Interfacial Tension, Mechanical Properties, Area/Molecule, and Permeability of fluid Lipid Bilayers. Biophys. J. **87**, 1013–1033 (2004).
59. McLaughlin, S.: Electrostatic Potentials at Membrane-Solution Interfaces. Curr. Top. Membr. Transp. **9**, 71–98 (1977).
60. Mengistu, D. H. and May, S.: Debye-Hückel theory of mixed charged-zwitterionic lipid layers. Eur. Phys. J. E **26**, 251–260 (2008).
61. Miloshevsky, G. V. and Jordan, P. C.: Gating gramicidin channels in lipid bilayers: reaction coordinates and the mechanism of dissociation. Biophys. J. **86**, 92–104 (2004).
62. Mobashery, N., Nielsen, C. and Andersen, O.S.: The conformational preference of gramicidin channels is a function of lipid bilayer thickness. FEBS Lett. 412, 15–20 (1997).
63. Mtheitsen, O. G. and Bloom, M.: Mattress model of lipid-protein interactions in membranes. Biophys. J. **46**, 141–153 (1984).

64. Mtheitsen, O. G. and Andersen, O.S.: In Biol. Skr. Dan. Vid. (Selsk Munksgaard, Copenhagen: B) (1998).
65. Muller, R. U. and Finkelstein, A.: The Effect of Surface Charge on the Voltage-Dependent Conductance Induced in Thin Lipid Membranes by Monazomycin. J. Gen. Physiol. **60**, 285–306 (1972).
66. Nielsen, C., Goulian, M. and Andersen, O.S.: Biophys, Energetics of inclusion-induced bilayer deformations, Biophys. J. **74**, 1966–1983 (1998).
67. Nielsen, C. and Andersen, O.S.: Inclusion-induced bilayer deformations: effects of monolayer equilibrium curvature. Biophys. J. **79**, 2583–2604 (2000).
68. O'Connell, A. M., Koeppe, R.E. II and Andersen, O.S.: Kinetics of gramicidin channel formation in lipid bilayers: trans-membrane monomer association. Science 250, 1256–1259 (1990).
69. Odijk, T.: Polyelectrolytes near the rod limit. J. Plym. Sci., Polym. Phys. Ed. 15, 477–483 (1977).
70. Orbach, E. and Finkelstein, A.: The nonelectrolyte permeability of planar lipid bilayer membranes. J. Gen. Physiol. **75**, 427–436 (1980).
71. Parsegian, A.: Energy of an Ion crossing a low dielectric membrane: solutions to fthe relevant electrostatic problems. Nature **221**, 844–846 (1969).
72. Perozo, E., Cortes, D.M. and Cuello, L.G.: Structural Rearrangements Underlying K^+- Channel Activation Gating. Science 285, 73–78 (1999).
73. Perozo, E., Cortes, D. M., Sompornpisut, P., Kloda, A. and Martinac, B.: Open channel structure of MscL and the gating mechanism of mechanosensitive channels. Nature **418**, 942–948 (2002).
74. Ring, A.: Gramicidin channel-induced lipid membrane deformation energy: influence of chain length and boundary conditions. Biochim. Biophys. Acta **1278**, 147–159 (1996).
75. Rostovtseva, T. K., Aguilella, V. M., Vodayanoy, I., Bezrukov, S. M. and Parsegian, A.: Membrane surface-charge titration probed by gramicidin A channel conductance. Biophys. J. **75**, 1783–1792 (1998).
76. Sackmann, E.: In Biological Membranes. Chapman, D. (ed.) (London: Academic), p 105 (1984).
77. Santore, M. M., Discher, D. E., Won, Y-Y., Bates, F. S. and Hammer, D. A.: Effect of Surfactant on Unilamellar Polymeric Vesicles: Altered Membrane Properties and Stability in the Limit of Weak Surfactant Partitioning. Langmuir **18**, 7299–7308 (2002).
78. Sawyer, D. B., Koeppe, R.E. II and Andersen, O.S.: Induction of conductance heterogeneity in gramicidin channels. Biochemistry **28**, 6571–6583 (1989).
79. Schatzberg, P. J.: Polymer Sci. Part C 10, 87–92 (1965).
80. Seddon, J. M.: Structure of the inverted hexagonal (H_{II}) phase, and non-lamellar phase transitions of lipids. Biochim. Biophys. Acta **1031**, 1–69 (1990).
81. Simon, S.A., McIntosh, T.J. and Latorre, R.: Influence of cholesterol on water permeation into bilayers. Science **216**, 65–67 (1982).
82. Singer, S.J. and Nicolson, G.L.: The fluid mosaic model of the structure of cell membranes. Science **175**, 720–731 (1972).
83. Szabo, G., Eisenman, G. and Ciani, S.: The effects of the macrotetralide actin antibiotics on the electrical properties of phospholipid bilayer membranes. J. Membr. Biol. 1, **346** (1969).
84. Tate, M. W., Eikenberry, E. F., Turner, D. C., Shyamsunder, E. and Gruner, S. M.: Nonbilayer phases of membrane lipids. Chem. Phys. Lipids **57**, 147–164 (1991).
85. Teh, C.K., Tuszynski, J. and Weisman, F.L.: The decay of carbon luminescence in liquid-encapsulated czochralski-grown semi-insulating GaAs. J. Mater. Res. **5**, 365–371 (1990).
86. Townsley, L. E., Tucker, W. A., Sham, S. and Hinton, J. F.: Structures of gramicidins A, B, and C incorporated into sodium dodecyl sulfate micelles. Biochemistry **40**, 11676–11686 (2001).
87. Toyoshima, C. and Mizutani, T.: Crystal structure of the calcium pump with a bound ATP analogue. Nature **430**, 529–535 (2004).
88. Unwin, P.N.T. and Ennis, P. D.: Two configurations of a channel-forming membrane protein. Nature **307**, 609–613 (1984).
89. Wallace, B. A., Veatch, W. R. and Blout, E. R.: Conformation of gramicidin A in phospholipid vesicles: circular dichroism studies of effects of ion binding, chemical modification, and lipid structure. Biochemistry **20**, 5754–5760 (1981).

90. Walter, A. and Gutknecht, J.: Monocarboxylic acid permeation through lipid bilayer membranes. J. Membrane Biol. **77**, 255–264 (1984).
91. Woolf, T.B. and Roux, B.: Molecular dynamics simulation of the gramicidin channel in a phospholipid bilayer. Proc. Natl. Acad. Sci. USA **91**, 11631–11635 (1994).
92. Wu, Y., He, K., Ludtke, S. J. and Huang, H. W.: X-ray diffraction study of lipid bilayer membranes interacting with amphiphilic helical peptides: diphytanoyl phosphatidylcholine with alamethicin at low concentrations. Biophys. J. **68**, 2361–2369 (1995).
93. Zhou, Y. and Raphael, R. M.: Effect of Salicylate on the Elasticity, Bending Stiffness, and Strength of SOPC Membranes. Biophys. J. **89**, 1789–1801 (2005).